NUMERICAL SOLUTION OF THE COMPRESSIBLE NAVIER-STOKES EQUATIONS USING DENSITY GRADIENTS AS ADDITIONAL DEPENDENT VARIABLES

by

Jang-Hyuk Kwon

A Thesis
Submitted to the Faculty of
Mississippi State University
in Partial Fulfillment of the Requirements
for the Degree of Master of Science
in the Department of Aerophysics and
Aerospace Engineering

Mississippi State, Mississippi

December, 1977

NUMERICAL SOLUTION OF THE COMPRESSIBLE NAVIER-STOKES EQUATIONS USING DENSITY GRADIENTS AS ADDITIONAL DEPENDENT VARIABLES

by

Jang-Hyuk Kwon

A Thesis
Submitted to the Faculty of
Mississippi State University
in Partial Fulfillment of the Requirements
for the Degree of Master of Science
in the Department of Aerophysics and
Aerospace Engineering

Mississippi State, Mississippi

December, 1977

NUMERICAL SOLUTION OF THE COMPRESSIBLE NAVIER-STOKES EQUATIONS

USING DENSITY GRADIENTS AS ADDITIONAL DEPENDENT VARIABLES

by

Jang-Hyuk Kwon

Approved:

Professor of Aerospace Engineering and Head, Department of Aerophysics and Aerospace Engineering	Director of Graduate Instruction, College of Engineering
Professor of Aerophysics and Areospace engineering (Major Professor)	Dean of the College of Engineering

Dean of the Graduate School

December, 1977

ACKNOWLEDGEMENT

At the moment of attaining a M.S. degree, the author wishes to express his thanks to Mr. Charles B. Cliett, Head of the Department of Aerophysics and Aerospace Engineering, for his support through the years, and to the entire department for their warm-heartedness and kindness.

Special thanks is due Dr. Joe F. Thompson as major professor, for his guidance and contribution to the author's education and his research effort.

Also, special thanks is due Mr. Louie Turner for his guidance and frequent assistance.

Thanks is also due Dr. Z. U. A. Warsi and Dr. A. G. Bennett, Jr., for their time and patience in correcting the author's thesis.

Finally, the author wishes to express his gratitude to his grandparents, parents and his whole family for their effort and unselfish sacrifice for him.

This research was supported in part by NASA, Langley Research Center, Grant NGR-25-001-055.

J. H. K.

Mississippi State University

December, 1977

ABSTRACT

Jang-Hyuk Kwon, Master of Science, 1977

Major: Aerospace Engineering, Department of Aerophysics and Aerospace Engineering

Title of Thesis: Numerical Solution of the Compressible Navier-Stokes Equations Using Density Gradients as Additional Dependent Variables

Directed by: Dr. Joe F. Thompson

Pages in Thesis: 75 Words in Abstract: 217

ABSTRACT

Numerical solution of two-dimensional, time-dependent, compressible viscous Navier-Stokes equations about arbitrary bodies is treated using density gradients as additional dependent variables. Thus, there are six dependent variables, ρ, u, v, E_s, ρ_x and ρ_y, to be computed with the SOR iteration method. Besides the new formulation for pressure gradient terms, a new formulation for computing the body density is presented. To approximate the governing equations, an implicit finite difference method is employed. The coordinate system used here is the automatically generated body-fitted coordinate system that was developed at Mississippi State University.

In computing the solution for the flow about a circular cylinder, a problem arose near the wall at both stagnation points. Thus, computations with various conditions were tried to examine the problem. Also, computations with and without new formulations are compared. The flow variables are computed on 37 by 40 field first, then on an 81 by 40 field.

As a result, density profiles are shown at different time steps with various conditions. Profiles for velocity and total energy, velocity vectors, Mach number contours and isobars are shown for particular cases.

Lastly, convective terms in transformed plane due to the coordinate stretching and the transformed velocity are introduced to conclude that the coordinate stretching plays an important role in this problem. Two ways of overcoming this problem are suggested.

TABLE OF CONTENTS

LIST OF SYMBOLS

Symbol	
A,D	Constants in transformed equations, Equation (3.10)
$\underline{A}$	Area vector, normal to its surface
$\bar{c}$	Body chord
$C_2, C_3, \ldots, C_{18}$	Coefficients defined in Table 3-1
$Cu_\eta, Cv_\eta, Ce_\eta$	Convective terms in transformed plane
E_s	Specific total energy
e	Internal energy
f,g	Scalar functions
F,G,U	Arrays of equations in vector form, Equation (3.9)
h	Enthalpy
h_1	Sutherland viscosity law reference temperature
J	Jacobian determinant
M	Mach number
p	Pressure
POA	Product of average
Pr	Prandtl number
P,Q	Functions which control the coordinate spacing
q_i	Heat flux
R	Reynolds number
Ra	Distances from the center of the circular cylinder
SOR	Successive-Over-Relaxation
T	Temperature
t	Time

u	Velocity component in x-direction
$\hat{u}$	Transformed velocity component in ξ-direction
v	Velocity component in y-direction
$\hat{v}$	Transformed velocity component in ξ-direction
$\hat{\underline{Y}}$	Transformed velocity vector
x,y	Physical coordinate
α,β,γ	Coordinate transformation parameter, in Table 3-1
Γ	Contour in physical plane
Γ^*	Contour in transformed plane
η,ξ	Transformed coordinates
η_1,η_2	Inner and outer boundary contours
Θ	Ratio of specific heats, c_p/c_v
λ	Second coefficient of viscosity
μ'	Bulk coefficient of viscosity
μ	First coefficient of viscosity
ρ	Density
σ_{xx},σ_{yy}	Normal stresses
τ_{xy},τ_{yx}	Shear stresses

Subscripts

i,j	Field position in (ξ,η) plane
t,x,y,η,ξ	First partial differentiation
$xx,yy,\eta\eta,\xi\xi$	Second partial differentiation
$xy,yx,\xi\eta$	Cross partial differentiation
w	Value on the wall
∞	Value of the freestream

Superscript

*	Denotes the transformed plane
n	Time step index
o	Initial value
°	Degrees

Prefix

Δ	Denotes increment
∂	Denotes partial differentiation
d	Denotes ordinary differentiation

I. INTRODUCTION

An implicit finite difference method is used to solve the two-dimensional, time-dependent, compressible viscous Navier-Stokes equations about arbitrary bodies using the body-fitted coordinate system. A new formulation for pressure gradient terms and body density is developed and solutions are compared with those with conventional formulations. Various computations are made using different conditions and different ways to examine the problem. The new formulation is developed because the wiggles which appear in the results with conventional formulation can be suppressed by using the density gradient method.

Usually, the compressible viscous flows have been solved by an explicit scheme, and an implicit scheme is rarely used. Moreover, the compressible viscous flows about a circular cylinder have been rarely solved. Recent works about the flows past a circular cylinder are these: [1] used polar coordinates to solve the steady incompressible Newtonian flows with low Reynolds numbers; in [2], impulsively started, time-dependent inviscid transonic flows were solved with different meshes, different freestream Mach numbers and Reynolds numbers; in [3], inviscid compressible supercritical flows were considered using polar coordinates. The explicit scheme was used in all these works.

II. BODY-FITTED COORDINATE SYSTEM

The basic idea of the body-fitted coordinate system is to generate the coordinate system having some coordinate line coincident with the boundary or body surface. A general method of generating body-fitted coordinate systems is to let the curvilinear coordinates to be solutions of an elliptic partial differential system in the physical plane with the Dirichlet boundary conditions on all boundaries. Thus, all the computations can be done on a rectangular field with a square mesh and all boundary conditions can be expressed at grid points, regardless of the body shape.

Major advantages of using body-fitted coordinates are; first, the computer software utilized to generate the body-fitted coordinate system is independent of the set of partial differential equations to be solved on this system; second, the computer software generated to approximate the solution of a given set of partial differential equations is completely independent of the physical geometry of the problem; finally, physical integral conservation relations need not be lost in the transformed plane [4]. This technique is extendable to three dimensions and applicable to fields with time-dependent boundaries.

Consider the transformation of a two-dimensional, doubly-connected region, R, bounded by two closed boundaries Γ_1 and Γ_2 onto a rectangular region, R^* as shown in Figure 1. The boundaries Γ_1 and Γ_2 in the physical plane are denoted by Γ_1^* and Γ_2^* in the transformed rectangular plane.

Let us consider taking Laplace's equation with inhomogeneous

terms on the right hand sides as the generating elliptic system. Then, these equations are:

$$\xi_{xx} + \xi_{yy} = P(\xi,\eta) \ , \tag{2.1a}$$

$$\eta_{xx} + \eta_{yy} = Q(\xi,\eta) \tag{2.1b}$$

with the Dirichlet boundary conditions

$$\begin{bmatrix} \xi \\ \\ \eta \end{bmatrix} = \begin{bmatrix} \xi_1(x,y) \\ \\ \eta_1 \end{bmatrix} \quad , \quad (x,y) \in \Gamma_1 \tag{2.1c}$$

$$\begin{bmatrix} \xi \\ \\ \eta \end{bmatrix} = \begin{bmatrix} \xi_2(x,y) \\ \\ \eta_2 \end{bmatrix} \quad , \quad (x,y) \in \Gamma_2 \tag{2.1d}$$

One coordinate is set to be constant on the body and the outer boundary, while the other is set to vary monotonically around the body.

In the transformed plane where all computations are made, the transformed equations are

$$\alpha x_{\xi\xi} - 2\beta x_{\xi\eta} + \gamma x_{\eta\eta} = - J^2 \left[x_\xi P(\xi,\eta) + x_\eta Q(\xi,\eta) \right] \tag{2.2a}$$

$$\alpha y_{\xi\xi} - 2\beta y_{\xi\eta} + \gamma x_{\eta\eta} = - J^2 \left[y_\xi P(\xi,\eta) + y_\eta Q(\xi,\eta) \right] \tag{2.2b}$$

where

$$\alpha \equiv x_\eta^2 + y_\eta^2 \tag{2.2c}$$

$$\beta \equiv x_\xi x_\eta + y_\xi y_\eta \tag{2.2d}$$

$$\gamma \equiv x_\xi^2 + y_\xi^2 \tag{2.2e}$$

with the boundary conditions

$$\begin{bmatrix} x \\ y \end{bmatrix} = \begin{bmatrix} f_1(\xi,\eta_1) \\ f_2(\xi,\eta_1) \end{bmatrix}, \quad (\xi,\eta_1) \in \Gamma_1^* \tag{2.2f}$$

$$\begin{bmatrix} x \\ y \end{bmatrix} = \begin{bmatrix} g_1(\xi,\eta_2) \\ g_2(\xi,\eta_2) \end{bmatrix}, \quad (\xi,\eta_2) \in \Gamma_2^* \tag{2.2g}$$

The functions $f_1(\xi,\eta_1)$, $f_2(\xi,\eta_1)$, $g_1(\xi,\eta_2)$ and $g_2(\xi,\eta_2)$ are specified by the known shape of the boundaries Γ_1 and Γ_2, and the distribution of ξ specified. Boundary data are not needed along the re-entrant boundaries Γ_3^* and Γ_4^*. The functions, $P(\xi,\eta)$ and $Q(\xi,\eta)$ are used for controlling the coordinate spacing.

The quasi-linear elliptic set of partial differential equations (2.2) are then solved on the rectangular transformed plane using finite differences and SOR iteration.

A detailed presentation of the coordinate generation method has been given in [4,5,6,7].

III. APPLICATION TO THE NAVIER-STOKES EQUATIONS IN PRIMITIVE VARIABLES

The body-fitted coordinate system is used to obtain numerical solutions of the two-dimensional, time-dependent, compressible viscous Navier-Stokes equations about arbitrary bodies. The conventional form of the governing equations from [8] is given first, then the new formulations for pressure gradients and body density are presented. In all equations, conservative forms are used.

A. Flow Equation Formulation — Conventional Form [8]

The primitive variable formulation of the two-dimensional, unsteady compressible viscous flow equations in a non-dimensional x,y coordinate system is given by

$$\frac{\partial \rho}{\partial t} + \frac{\partial (\rho u)}{\partial x} + \frac{\partial (\rho v)}{\partial y} = 0 \tag{3.1a}$$

$$\frac{\partial (\rho u)}{\partial t} + \frac{\partial (\rho u^2)}{\partial x} + \frac{\partial (\rho uv)}{\partial y} = \frac{\partial \sigma_{xx}}{\partial x} + \frac{\partial \tau_{yx}}{\partial y} \tag{3.1b}$$

$$\frac{\partial (\rho v)}{\partial t} + \frac{\partial (\rho vu)}{\partial x} + \frac{\partial (\rho v^2)}{\partial y} = \frac{\partial \tau_{xy}}{\partial x} + \frac{\partial \sigma_{yy}}{\partial y} \tag{3.1c}$$

$$\frac{\partial E_s}{\partial t} + \frac{\partial (E_s u)}{\partial x} + \frac{\partial (E_s u)}{\partial y} = (\Theta - 1)M_\infty^2 \left[\frac{\partial}{\partial x}(\sigma_{xx} u + \tau_{xy} v) + \frac{\partial}{\partial y}(\tau_{yx} u + \sigma_{yy} v) \right]$$

$$+ \left(\frac{\Theta}{Pr \cdot R} \right) \left[\frac{\partial}{\partial x} \left(\mu \frac{\partial e}{\partial x} \right) + \frac{\partial}{\partial y} \left(\mu \frac{\partial e}{\partial y} \right) \right] \tag{3.1d}$$

where

$$E_s = \rho [e + (\Theta - 1)M_\infty^2 (V^2/2)] \tag{3.2}$$

Θ, M_∞ and Pr are the ratio of heat, the freestream Mach number and the Prandtl number, respectively. The lengths or distances are non-dimensional with repect to the body chord, $\bar{c}$; time is non-dimensional with repect to the time required for passing one chord distance with the freestream velocity; density is non-dimensional with respect to the freestream density, ρ_∞; the velocity component u, v are non-dimensional with respect to the magnitude of the freestream velocity, V_∞; the thermodynamic variable, the internal energy, e, is non-dimensional with respect to the static enthalpy of the freestream, h_∞; and the thermodynamic variables of pressure and the total energy, E_s, are non-dimensional with respect to the product of the freestream density and the static enthalpy of the freestream, $\rho_\infty h_\infty$. The Prandtl number, Pr, is the product of viscosity and specific heat at constant pressure divided by thermal conductivity. Components of stress tensor are non-dimensional with respect to $\rho_\infty V_\infty^2$ and are given by

$$\sigma_{xx} = -\frac{P}{(\Theta - 1)M_\infty^2} + \frac{\lambda}{R}\left(\frac{\partial u}{\partial x} + \frac{\partial v}{\partial y}\right) + \frac{\mu}{R}\left(2\,\frac{\partial u}{\partial x}\right) \tag{3.3a}$$

$$\sigma_{yy} = -\frac{P}{(\Theta - 1)M_\infty^2} + \frac{\lambda}{R}\left(\frac{\partial u}{\partial x} + \frac{\partial v}{\partial y}\right) + \frac{\mu}{R}\left(2\,\frac{\partial v}{\partial y}\right) \tag{3.3b}$$

$$\tau_{xy} = \tau_{yx} = \frac{\mu}{R}\left(\frac{\partial v}{\partial x} + \frac{\partial u}{\partial y}\right) \tag{3.3c}$$

with

$$\lambda \equiv \mu' - 2\mu/3 \quad \text{and} \quad R \equiv \rho_\infty V_\infty \bar{c}/\mu_\infty$$

The Reynolds number, R, is based on freestream conditions and the body chord, $\bar{c}$. Bulk viscosity, μ' is approximately zero in the

case of local thermodynamic equilibrium which is assumed to be the case in the present investigation.

Additional relations are needed to solve the compressible flow equations. They are the equations of state and a relation for the viscosity.

$$p = (\Theta - 1)\rho e \tag{3.4}$$

$$\mu = (h)^{3/2}\left[(1 + h_1)/(h + h_1)\right] \tag{3.5}$$

In the Sutherland viscosity law, (3.5), h_1 is a constant, whose value depends on the type of gas, and the non-dimensional enthalpy, h, equals the product of specific heat ratio, Θ, and internal energy, e.

Boundary Conditions

The boundary conditions on the body surface are;

$$u = v = 0 \tag{3.6a}$$

and

$$T_w = \text{constant} \tag{3.6b}$$

or

$$q_i = 0 \quad \text{(adiabatic wall)} \tag{3.6c}$$

The wall temperature, T_w, is non-dimensional with repect to the stagnation temperature of the freestream.

Far from the body, the boundary conditions are

$$\rho = 1 \qquad \text{at infinity} \tag{3.7a}$$

$$u = 1 \ , \quad v = 0 \qquad \text{at infinity} \qquad (3.7b)$$

$$E_s = \frac{1}{\Theta} + \frac{(\Theta - 1)M_\infty^2}{2} \qquad \text{at infinity} \qquad (3.7c)$$

Transformed Equations

After transforming to the body-fitted coordinates (ξ,η), using the transformation relations of Appendix A of [4], the governing equations (3.1) can be written in the vector form [8].

$$\frac{\partial U}{\partial t} + \frac{\partial F}{\partial \xi} + \frac{\partial G}{\partial \eta} = 0 \qquad (3.8)$$

The ordered arrays U, F, and G are:

$$U = \begin{pmatrix} J\rho \\ J\rho u \\ J\rho v \\ JE_s \end{pmatrix} \qquad (3.9a)$$

$$F = \begin{pmatrix} \rho\hat{u} \\ \rho u\hat{u} + \tau_{yx}x_\eta - \sigma_{xx}y_\eta \\ \rho v\hat{u} + \sigma_{yy}x_\eta - \tau_{xy}y_\eta \\ E_s\hat{u} + D\,\tau_{yx}x_\eta - \sigma_{xx}y_\eta\, u + D\,\sigma_{yy}x_\eta - \tau_{xy}y_\eta\, v - A\,e_x y_\eta - e_y x_\eta \end{pmatrix} \qquad (3.9b)$$

$$G = \begin{pmatrix} \rho\hat{v} \\ \rho u\hat{v} + \sigma_{xx}y_\xi - \tau_{yx}x_\xi \\ \rho v\hat{v} + \tau_{xy}y_\xi - \sigma_{yy}x_\xi \\ E_s\hat{v} + D\,\sigma_{xx}y_\xi - \tau_{yx}x_\xi\, u + D\,\tau_{xy}y_\xi - \sigma_{yy}x_\xi\, v - A\,e_y x_\xi - e_x y_\xi \end{pmatrix} \qquad (3.9c)$$

where

$$D = (\Theta - 1)M_\infty^2 \qquad A = \frac{\Theta\mu}{Pr \cdot R} \qquad (3.10)$$

Transformed velocity components $\hat{u}$, $\hat{v}$ are defined below, and J is the Jacobian of the transformation : $J = x_\xi y_\eta - x_\xi y_\eta$,

$$\hat{u} = uy_\eta - vx_\eta \quad , \quad \hat{v} = vx_\xi - uy_\xi \tag{3.11}$$

The transformed forms of stress terms are given in equations (3.12), (3.13), (3.14), respectively.

$$\tau_{yx}x_\eta - \sigma_{xx}y_\eta = \frac{py_\eta}{D} - \frac{\mu}{R}\left[c_9 u_\xi - c_{13}u_\eta - c_{16}v_\xi + c_{18}v_\eta\right] \tag{3.12a}$$

$$\sigma_{xx}y_\xi - \tau_{yx}x_\xi = -\frac{py_\xi}{D} + \frac{\mu}{R}\left[c_{13}u_\xi - c_{11}u_\eta - c_{17}v_\xi + c_{15}v_\eta\right] \tag{3.12b}$$

$$\sigma_{yy}x_\eta - \tau_{xy}y_\eta = -\frac{px_\eta}{D} + \frac{\mu}{R}\left[c_{16}u_\xi - c_{17}u_\eta - c_{10}v_\xi + c_{14}v_\eta\right] \tag{3.12c}$$

$$\tau_{xy}y_\xi - \sigma_{yy}x_\xi = \frac{px_\xi}{D} + \frac{\mu}{R}\left[c_{18}u_\xi - c_{15}u_\eta - c_{14}v_\xi + c_{12}v_\eta\right] \tag{3.12d}$$

$$\begin{aligned}(\tau_{yx}x_\eta - \sigma_{xx}y_\eta)u + (\sigma_{yy}x_\eta - \tau_{xy}y_\eta)v = \frac{p\hat{u}}{D} - \frac{\mu}{R}\Big[&(c_9 u - c_{16}v)u_\xi \\ &+ (c_9 v - c_{13}u)u_\eta + (c_{18}u - c_{14}v)v_\eta \\ &+ (c_{10}v - c_{16}u)v_\xi\Big]\end{aligned} \tag{3.13a}$$

$$\begin{aligned}(\sigma_{xx}y_\xi - \tau_{yx}x_\xi)u + (\tau_{xy}y_\xi - \sigma_{yy}x_\xi)v = \frac{p\hat{v}}{D} + \frac{\mu}{R}\Big[&(c_{13}u - c_{18}v)u_\xi \\ &+ (c_{15}v - c_{11}u)u_\eta + (c_{15}u - c_{12}v)v_\eta \\ &+ (c_{14}v - c_{17}u)v_\xi\Big]\end{aligned} \tag{3.13b}$$

$$e_x y_\eta - e_y x_\eta = c_2 e_\xi - c_3 e_\eta \tag{3.14a}$$

$$e_y x_\xi - e_x y_\xi = c_4 e_\eta - c_3 e_\xi \tag{3.14b}$$

The subscripted coefficients c are defined in Table 3 - 1 with the definitions of α, β, and γ. Those coefficients missing from the table, e. g., c_1, arise in the differencing of the transformed equations.

TABLE 3 - 1. Coefficients For Transformed Equations

$c_2 = \alpha/J$	$c_{14} = (3\beta + x_\xi x_\eta)/3J$
$c_3 = \beta/J$	$c_{15} = x_\xi y_\xi/3J$
$c_4 = \gamma/J$	$c_{16} = x_\eta y_\eta/3J$
$c_9 = (3\alpha + y_\eta^2)/3J$	$c_{17} = (x_\xi y_\eta - 2J)/3J$
$c_{10} = (3\alpha + x_\eta^2)/3J$	$c_{18} = (x_\eta y_\xi - 2J)/3J$
$c_{11} = (3\gamma + y_\xi^2)/3J$	$\alpha = x_\eta^2 + y_\eta^2$
$c_{12} = (3\gamma + x_\xi^2)/3J$	$\beta = x_\xi x_\eta + y_\xi y_\eta$
$c_{13} = (3\beta + y_\xi y_\eta)/3J$	$\gamma = x_\xi^2 + y_\xi^2$

Solution of the equations (3.8) through (3.14) uses the equation of state given by (3.4), the viscosity law given by (3.5) and the boundary conditions given by (3.6) and (3.7). There is no change in these equations for flow solutions in the body-fitted coordinate system.

B. New Formulation of Flow Equations

Generally, the pressure gradient terms in transformed momentum equations are computed by using the equation of state for pressure values and central difference approximations for derivatives.

New formulations for computing the pressure gradient terms and the body density are discussed below.

Formulation of Equations for Pressure Gradients

The equations of state (3.4) is used and differentiated as a whole with respect to x and y to get the pressure gradient terms. Thus, the pressure gradient terms of x and y momentum equations in (3.1) and (3.3) can be replaced by

$$\frac{\partial p}{\partial x} = (\theta - 1)\left[\rho \frac{\partial e}{\partial x} + e \frac{\partial \rho}{\partial x}\right] \tag{3.15a}$$

$$\frac{\partial p}{\partial y} = (\theta - 1)\left[\rho \frac{\partial e}{\partial y} + e \frac{\partial \rho}{\partial y}\right] \tag{3.15b}$$

The transformed derivatives of internal energy are expressed as below. The internal energy at each point can be calculated from the energy equation.

$$\frac{\partial e}{\partial x} = \frac{1}{J}\left[y_\eta e_\xi - y_\xi e_\eta\right] \tag{3.16a}$$

$$\frac{\partial e}{\partial y} = \frac{1}{J}\left[x_\xi e_\eta - x_\eta e_\xi\right] \tag{3.16b}$$

To get ρ_x and ρ_y in (3.15), two equations are obtained from the continuity equation by differentiation with respect to x and y, respectively:

$$\frac{\partial \rho_x}{\partial t} = - \frac{\partial^2(\rho u)}{\partial x^2} - \frac{\partial^2(\rho v)}{\partial x \partial y} \tag{3.17a}$$

$$\frac{\partial \rho_y}{\partial t} = - \frac{\partial^2(\rho u)}{\partial y \partial x} - \frac{\partial^2(\rho v)}{\partial y^2} \tag{3.17b}$$

After transformation, the following expressions for ρ_x and ρ_y are obtained.

$$\frac{\partial \rho_x}{\partial t} = - \text{RUDXX} - \text{RVDXY} \tag{3.18a}$$

$$\frac{\partial \rho_y}{\partial t} = - \text{RUDYX} - \text{RVDYY} \tag{3.18b}$$

where

$$\text{RUDXX} = \left(\frac{y_\eta}{J}\right) \frac{\partial}{\partial \xi} \left\{ \frac{y_\eta}{J}(\rho u)_\xi - \frac{y_\xi}{J}(\rho u)_\eta \right\} - \left(\frac{y_\xi}{J}\right) \frac{\partial}{\partial \eta} \left\{ \frac{y_\eta}{J}(\rho u)_\xi - \frac{y_\xi}{J}(\rho u)_\eta \right\} \tag{3.18c}$$

$$\text{RVDXY} = \left(\frac{y_\eta}{J}\right) \frac{\partial}{\partial \xi} \left\{ \frac{x_\xi}{J}(\rho v)_\eta - \frac{x_\eta}{J}(\rho v)_\xi \right\} - \left(\frac{y_\xi}{J}\right) \frac{\partial}{\partial \eta} \left\{ \frac{x_\xi}{J}(\rho v)_\eta - \frac{x_\eta}{J}(\rho v)_\xi \right\} \tag{3.18d}$$

$$\text{RUDYX} = \left(\frac{x_\xi}{J}\right)\frac{\partial}{\partial\eta}\left\{\frac{y_\eta}{J}(\rho u)_\xi - \frac{y_\xi}{J}(\rho u)_\eta\right\} - \left(\frac{x_\eta}{J}\right)\frac{\partial}{\partial\xi}\left\{\frac{y_\eta}{J}(\rho u)_\xi - \frac{y_\xi}{J}(\rho u)_\eta\right\} \tag{3.18e}$$

$$\text{RVDYY} = \left(\frac{x_\xi}{J}\right)\frac{\partial}{\partial\eta}\left\{\frac{x_\xi}{J}(\rho v)_\eta - \frac{x_\eta}{J}(\rho v)_\xi\right\} - \left(\frac{x_\eta}{J}\right)\frac{\partial}{\partial\xi}\left\{\frac{x_\xi}{J}(\rho v)_\eta - \frac{x_\eta}{J}(\rho v)_\xi\right\} \tag{3.18f}$$

Thus, ρ_x and ρ_y can be obtained from the finite difference version of the following equations.

$$\frac{(\rho_x)^n_{i,j} - (\rho_x)^{n-1}_{i,j}}{\Delta t} = -\,\text{RUDXX}\big|^n_{i,j} - \text{RVDXY}\big|^n_{i,j} \tag{3.19a}$$

$$\frac{(\rho_y)^n_{i,j} - (\rho_y)^{n-1}_{i,j}}{\Delta t} = -\,\text{RUDYX}\big|^n_{i,j} - \text{RVDYY}\big|^n_{i,j} \tag{3.19b}$$

After dropping the superscript n and denoting the superscript (n-1) by o,

$$(\rho_x)_{i,j} = (\rho_x)^o_{i,j} - \Delta t\left[\text{RUDXX}\big|_{i,j} + \text{RVDXY}\big|_{i,j}\right] \tag{3.20a}$$

$$(\rho_y)_{i,j} = (\rho_y)^o_{i,j} - \Delta t\left[\text{RUDYX}\big|_{i,j} + \text{RVDYY}\big|_{i,j}\right] \tag{3.20b}$$

ρ_x and ρ_y are treated as new dependent variables which change with

time. They are solved with the same procedure as the other dependent variables, ρ, u, v and E_s, using the SOR iteration method.

Thus, the pressure gradients, p_x and p_y, in (3.15) can be obtained directly using the equations (3.16) and (3.20) for the computations of e_x, e_y, ρ_x and ρ_y, rather than by differencing the pressure. Then, the momentum equations in (3.1) are changed as follows :

$$\frac{\partial(\rho u)}{\partial t} + \frac{\partial(\rho u^2)}{\partial x} + \frac{\partial(\rho uv)}{\partial y} = -\frac{1}{D}\frac{\partial p}{\partial x} + \frac{\partial \sigma'_{xx}}{\partial x} + \frac{\partial \tau_{yx}}{\partial y} \tag{3.21a}$$

$$\frac{\partial(\rho v)}{\partial t} + \frac{\partial(\rho vu)}{\partial x} + \frac{\partial(\rho v^2)}{\partial v} = -\frac{1}{D}\frac{\partial p}{\partial y} + \frac{\partial \tau_{xy}}{\partial x} + \frac{\partial \sigma'_{yy}}{\partial y} \tag{3.21b}$$

where

$$\sigma'_{xx} = \frac{\lambda}{R}\left(\frac{\partial u}{\partial x} + \frac{\partial v}{\partial y}\right) + \frac{\mu}{R}\left(2\frac{\partial u}{\partial x}\right) \tag{3.22a}$$

$$\sigma'_{yy} = \frac{\lambda}{R}\left(\frac{\partial u}{\partial x} + \frac{\partial v}{\partial y}\right) + \frac{\mu}{R}\left(2\frac{\partial v}{\partial y}\right) \tag{3.22b}$$

The rest are all same as (3.1), (3.2) and (3.3). In transformed equations, (3.15) is used for pressure gradients, and σ'_{xx} and σ'_{yy} are used instead of σ_{xx} and σ_{yy}.

Other relations and boundary conditions are the same. When iterating for u and v, the terms p_x and p_y are computed using the most recent iterate values of ρ_x, ρ_y and e_x, e_y.

Formulation of Equations for Body Density

To compute the body density, either the continuity equation, or momentum equations evaluated on the body, or some type of the extrapolation method has commonly been used. Here, another way of computing the body density is presented by using the values of ρ_x and ρ_y computed above from (3.20).

In the transformed plane, ρ_x and ρ_y are expressed as

$$\rho_x = \frac{1}{J} [y_\eta \rho_\xi - y_\xi \rho_\eta] \tag{3.23a}$$

$$\rho_y = \frac{1}{J} [-x_\eta \rho_\xi + x_\xi \rho_\eta] \tag{3.23b}$$

From these equations, (3.23a) and (3.23b), multiplied by x_η and y_η respectively, the following relation can be derived.

$$\rho_\eta = x_\eta \rho_x + y_\eta \rho_y \tag{3.24}$$

Thus, ρ_η is expressed by a function of ρ_x and ρ_y. Now, ρ_η can be expressed as below using the second order central difference approximation.

$$\rho_\eta|_{i,2} = \frac{1}{2} [\rho_{i,3} - \rho_{i,1}] \tag{3.25}$$

This gives the body density in the form of

$$\rho_{i,1} = \rho_{i,3} - 2\, \rho_\eta|_{i,2} \tag{3.26a}$$

or,

$$\rho_{i,1} = \rho_{i,3} - 2\left[x_\eta \rho_x + y_\eta \rho_y\right]\Big|_{i,2} \qquad (3.26b)$$

Equation (3.26b) is used for the body density with $\rho_\eta|_{i,2}$ calculated by the equation (3.24) with the most recent iterate values of $(\rho_x)_{i,2}$ and $(\rho_y)_{i,2}$. Again, the SOR technique is used to compute the body density.

In the new formulation of flow equations, the pressure gradient terms are not represented by pressure differences, but are evaluated directly by using the values of energy gradients and density gradients.

IV. NUMERICAL FORMULATION

All space derivatives in the field are approximated by the second-order, central difference expressions. Thus, the first and second derivatives are approximated as below setting $\Delta\xi$ and $\Delta\eta$ to be unity.

$$(f_\xi)_{i,j} \triangleq \frac{1}{2}(f_{i+1,j} - f_{i-1,j}) \tag{4.1}$$

$$(f_\eta)_{i,j} \triangleq \frac{1}{2}(f_{i,j+1} - f_{i,j-1}) \tag{4.2}$$

$$(f_{\xi\xi})_{i,j} \triangleq f_{i+1,j} - 2f_{i,j} + f_{i-1,j} \tag{4.3}$$

$$(f_{\eta\eta})_{i,j} \triangleq f_{i,j+1} - 2f_{i,j} + f_{i,j-1} \tag{4.4}$$

$$(f_{\xi\eta})_{i,j} \triangleq \frac{1}{4}(f_{i+1,j+1} - f_{i+1,j-1} - f_{i-1,j+1} + f_{i-1,j-1}) \tag{4.5}$$

At the body surface, where central difference approximations can not be used for the derivatives with respect to η, the second- order, one-sided difference expressions are used.

$$(f_\eta)_{i,1} \triangleq \frac{1}{2}(-f_{i,3} + 4f_{i,2} - 3f_{i,1}) \tag{4.6}$$

In the ξ-directions, the central difference expressions are also used.

All the time derivatives are approximated by the first-order, backward difference expressions to get the implicit formulation.

$$(f_t)^n_{i,j} \cong \frac{f^n_{i,j} - f^{n-1}_{i,j}}{\Delta t} \tag{4.7}$$

The explicit method was not used because with explicit method, the elliptic character of spatial variation is totally neglected. Moreover, explicit methods have severe stability limitations [5].

Thus, the implicit formulation is used to solve the Navier-Stokes equations, and the set of resulting simultaneous difference equations with the boundary conditions are solved at each time step by the point SOR iteration.

For convenience sake, the finite difference equations for pressure gradient terms and body density are explained briefly in Chapter III. All other equations in difference expressions are as in [8].

V. RESULTS AND DISCUSSION

The case considered here is the flow about a circular cylinder at a freesream Reynolds number of 1000. The Mach number and the static temperature of the freestream were 0.8 and 273°K, respectively. The Prandtl number was set at 0.71 [9], and the viscosity law reference temperature, h_1 in (3.5), was 0.40293 [10]. For an initial solution, the incompressible potential flow solution was used. The field acceleration parameters were varied, but the convergence tolerance for all variables were set at 0.00001. The time steps used here were all 0.01, except in the runs of 3.

Runs were made on two different size fields; 37 by 40 field and 81 by 40 field, so the number of ξ-lines was increased later as shown in Figure 2 and 3. The field radius was 6.0 in either field. Log attraction was used to locate 25 lines inside the R=20 boundary layer in Figure 2 and 17 lines inside the R=106 boundary layer in Figure 3 by using [11].

As soon as the first run with the new formulation for pressure gradient terms and the continuity equation for the body density was made, dips and spikes showed up near the wall and developed as can be seen in Figure 4 and 5.

All the computations except 6, were made with the new formulation for pressure gradient terms and all the computations, except 1 and 6, were made by using the new formulation for body density. The adiabatic wall was assumed in all cases except run 4.

A. Computations Made with Various Conditions

On 37 by 40 Field

1. Computation with the Continuity Equation for Body Density

At first, the new formulation was substituted for the pressure gradient terms in the conventional formulation. The continuity equation evaluated at the wall was used for the body density as in [8]. The acceleration parameters for density, velocity, total energy, ρ_x and ρ_y were 0.95, 0.50, 0.80, 0.40 and 0.50, respectively. The acceleration parameters were set at 0.30 for body density and 1.0 for free-stream variables.

As soon as two time steps($t = 0.02$) passed, dips and spikes appeared in density profile and developed as the time proceeded. The density profiles are shown in Figure 4 and 5. Near the front stagnation point($\xi = 28$ line), the problem seems to be more serious than near the rear stagnation point($\xi = 10$ line).

2. Computation with the New Formulation for Body Density

The new formulation for body density was tried from this computation to the end, except the computation 6. Other conditions were the same as those of run 1. The density profiles are shown in Figure 6 and 7. Runs were made up to 1.0 in non-dimensional time. The profiles look better than those of run 1. The dips near the rear stagnation point became smaller as the time passed, but not small enough. Near the front stagnation point, the spikes developed and the differences of the values between the wall and the next point remained almost the same.

3. Computations with Different Time Steps

Time steps of 0.02 and 0.005 were tried using same conditions of run 2. As shown in Figure 8, 9 and 10, the results were almost same as that of run 2. The acceleration parameter of 1.0 was used for body density.

4. Computation with a Constant Wall Temperature

Instead of the adiabatic wall, the constant temperature wall was assumed. The time step was 0.01 and still the new formulations for pressure gradient terms and body density were used. Other conditions were the same as those of run 3. Wall temperatures were fixed at 1.0. As can be seen in Figure 11, the results became even worse. The values of body density went down at both stagnation points.

On 81 by 40 Field

5. Computation with New Formulations

The coordinate system was changed so as to get smaller grid sizes in ξ direction. The time step was 0.01 and acceleration parameters for density, velosity, total energy, ρ_x, ρ_y and body density were 0.95, 0.70, 0.80, 0.70, 0.60 and 1.0, respectively. The density profiles are shown in Figure 12 and 13. As can be seen from the figures, the dips were even worse than those of run 2 which was made on the 37 by 40 field with the same conditions. Still there are no oscillation except the dips and spikes. As the time passes, the dips remain almost same near the front stagnation point(ξ = 61 line) and slightly increasing near the rear stagnation point(ξ = 21 line).

In Figure 14 and 15, velocity profiles and total energy profiles

are shown. From the figures, it can be observed that the velocity profiles near the stagnation points are smooth and have no dips while the other have dips. Also, in Figure 16, the velocity vectors are shown near the front stagnation point. Applying the continuity equation in difference form to a point (61,2), lying next to the front stagnation point to η-direction, then it is easy to see that the outflow to η-direction is much more than the inflow, so that makes the density at this point go down.

6. Computation with Conventional Formulations [8]

For making a comparison with new formulations, the formulation of [8] was run at the condition of run 5. As can be seen in Figure 17 and 18, the density profiles look better near the wall than those of run 5 and other portions of density profiles are same. The oscillations near the wall occur in this computation, but not in the computation with the new formulations. When time is 1.0, the oscillations still exist near the wall though they are small. They are shown up to more than five cell width, sometimes more than ten cell width. But the sizes of the oscillations can be considered as a constant.

The computer time required was slightly more than a half of run 5. The acceleration parameters for density, velocity, total energy and body density used were 0.95, 0.70, 0.70 and 0.50, respectively.

The velocity vector plots with new formulations on 37 by 40 field and 81 by 40 field are shown in Figure 19 and 20, respectively. In Figure 21, the velocity vector plots with conventional formulations are shown. In the rear region, the formulations of circulating eddies can be seen. In the plot with new formulations on 81 by 40 field, waves

appeared. They appeared to be related to shock waves and velocity vectors oscillate near the waves. In Figure 22 and 23, Mach number contours and isobars are shown for the waves. From a study of the Mach number contours, it looks that shock waves will later be formed. The Mach number downstream of the waves are too high for these waves to be true shocks. Isobars are so close to each other near the waves. In plots with new formulations on 37 by 40 field and with conventional formulations on 81 by 40 field, the waves are smeared out.

7. Computation with Reynolds Number of 50

The density profiles are shown in Figure 24. New formulations for pressure gradient terms and body density were used with same conditions as run 5. This computation was made up to time of 0.1 to see whether the viscosity can cure the problem or not. As can be seen in the figure, dips and spikes are smoothed out.

B. Convection Terms Check

Besides the runs with various conditions, the convection terms were examined. At first, the expanded forms of convection terms in x and y momentum equations were used to check which terms are changed by the expanded forms. The expanded form used here is, for example, as below.

$$\frac{\partial (uv)}{\partial x} = u \frac{\partial v}{\partial x} + v \frac{\partial u}{\partial x}$$

All the terms that were calculated with and without using the expanded forms were computed. As a result, the changes in convection terms

near the stagnation points were pretty big. Thus, two changes below were tried to correct the problem.

1. Averages in the Continuity Equation

The continuity equation in integral form is

$$\iint \rho_t J \, d\xi d\eta = - \int \rho \hat{\underset{\sim}{V}} \cdot d\underset{\sim}{A} \tag{5.1}$$

where $\hat{\underset{\sim}{V}}$ is the transformed velocity expressed by $\hat{\underset{\sim}{V}} = \hat{u}\underset{\sim}{i} + \hat{v}\underset{\sim}{j}$.

The integral equation can be approximated as below:

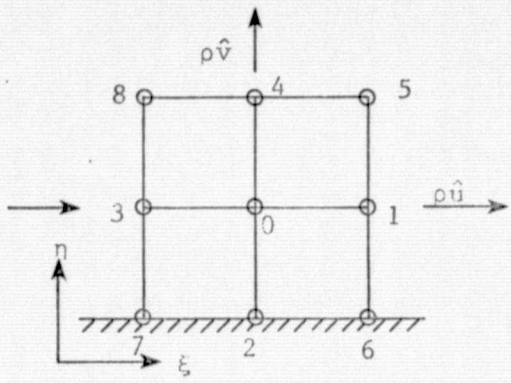

$$(4\rho_t J)_0 = -\left[\frac{(\rho\hat{u})_5+(\rho\hat{u})_1}{2} + \frac{(\rho\hat{u})_1+(\rho\hat{u})_6}{2}\right] + \left[\frac{(\rho\hat{u})_8+(\rho\hat{u})_3}{2} + \frac{(\rho\hat{u})_3+(\rho\hat{u})_7}{2}\right] - \left[\frac{(\rho\hat{v})_5+(\rho\hat{v})_4}{2} + \frac{(\rho\hat{v})_4+(\rho\hat{v})_8}{2}\right] + \left[\frac{(\rho\hat{v})_6+(\rho\hat{v})_2}{2} + \frac{(\rho\hat{v})_2+(\rho\hat{v})_7}{2}\right]$$

In this way, ρ_t was calculated to get ρ_0, but the result was even worse and densities went down more.

2. POA Forms

The product of average forms were tried in the continuity equation and x and y momentum equations and used only at the front and

rear stagnation point because the POA form can approximate better in the flow reversal region. But there were only very small changes in flow variables or no change at all.

C. Cu_η, Cv_η and Ce_η

From the results of various computations and the convection terms check, the following conclusions can be drawn :

1. The problem of dips and spikes is not an instability problems because at later time the magnitudes of dips remain almost same. Instability usually means oscillations and a rapid growth of errors.

2. There are truncation errors in computations near the stagnation points, but those are not due to the difference expressions of derivatives because the errors remained nearly constant when the cell size in ξ direction was reduced.

From [8], Cu_η, Cv_η and Ce_η are introduced as below by taking dominant terms in x and y momentum equations and energy equation near the stagnation point :

$$Cu_\eta = \frac{1}{R}\frac{\partial(\mu c_{11})}{\partial \eta} - \rho\hat{v} \tag{5.2}$$

$$Cv_\eta = \frac{1}{R}\frac{\partial(\mu c_{12})}{\partial \eta} - \rho\hat{v} \tag{5.3}$$

$$Ce_\eta = \frac{\Theta}{Pr \cdot R}\frac{\partial(\mu c_4)}{\partial \eta} - \rho\hat{v} \tag{5.4}$$

Where c_{11}, c_{12} and c_4 are shown in Table 3 - 1. These terms act like convective terms in the transformed plane. The first terms are due

to the coordinate streching in η direction and the second terms are due to the transformed velocity. Because dips are in density profiles and energy profiles, Ce_η is calculated as in Table 5 - 1 and ρe profiles are shown in Figure 25. The calculations were made with new formulations at t = 1.0.

TABLE 5-1. Ce_η

I	J	Ce_η	$-\rho\hat{v}$
62	1	-2.142×10^{-4}	0
	2	3.341×10^{-4}	5.060×10^{-4}
	3	1.824×10^{-3}	1.970×10^{-3}
	4	4.014×10^{-3}	4.158×10^{-3}
	5	6.652×10^{-3}	6.803×10^{-3}
	6	9.542×10^{-3}	9.702×10^{-3}
67	1	-2.135×10^{-4}	0
	2	2.110×10^{-4}	4.081×10^{-4}
	3	1.372×10^{-3}	1.548×10^{-3}
	4	3.053×10^{-3}	3.209×10^{-3}
	5	5.051×10^{-3}	5.198×10^{-3}
	6	7.243×10^{-3}	7.388×10^{-3}
71	1	-2.024×10^{-4}	0
	2	-6.198×10^{-5}	1.874×10^{-4}
	3	4.160×10^{-4}	6.574×10^{-4}
	4	1.037×10^{-3}	1.223×10^{-3}
	5	1.557×10^{-3}	1.782×10^{-3}
	6	2.431×10^{-3}	2.560×10^{-3}

Near or on the body surface, the first term is dominant while in the other region, the second term is dominant. In [8], the region where the first term is dominant is wider than this case because in his case the Reynolds number is much higher. In Figure 23, the ρe profiles are not realistic, too.

From these calculations, it can be said that the coordinate stretching makes the problem, or, at least, plays an important role

in the problem.

In regions of large gradients, a fine mesh is usually used. In [12, 13], halving the coarse mesh cell size was used to get a medium mesh and a fine mesh, and the governing equations were solved separately. In [14], a fine, exponentially stretched mesh spacing was employed and explicit artificial viscosity terms were added to avoid the instability. In [15, 16], the same stretched coordinate spacing as [14] was used but a fine constant mesh spacing was used in the sublayer region.

VI. CONCLUSION

An implicit finite difference method was applied to solve the compressible viscous flows about a circular cylinder using new formulations for pressure gradient terms and the body density, but a problem arose near the stagnation points in both results with and without the new formulations. In the result with conventional formulation [8], wiggles appear near the wall, but not in the results with new formulations, except the dips and spikes. It was concluded that the coordinate stretching in the η-direction plays an important role on the truncation errors which causes the problem.

This problem can be corrected by; 1) employing explicit artificial viscosity terms, or 2) employing a few η lines which have a constant or very slowly changing spacing for a first few η lines.

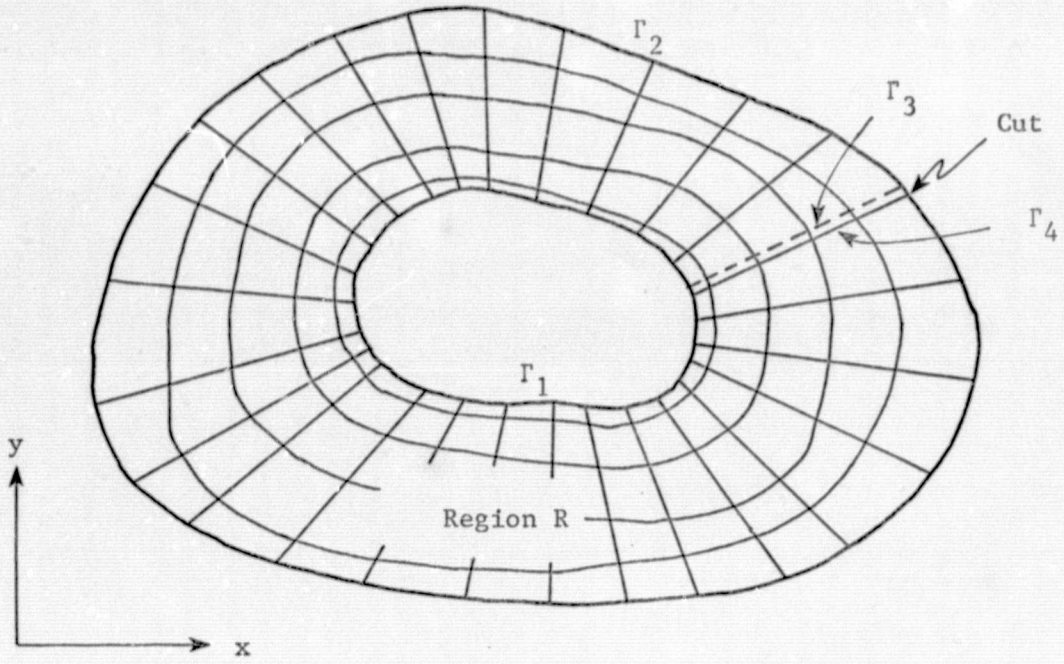

(a) Physical Plane

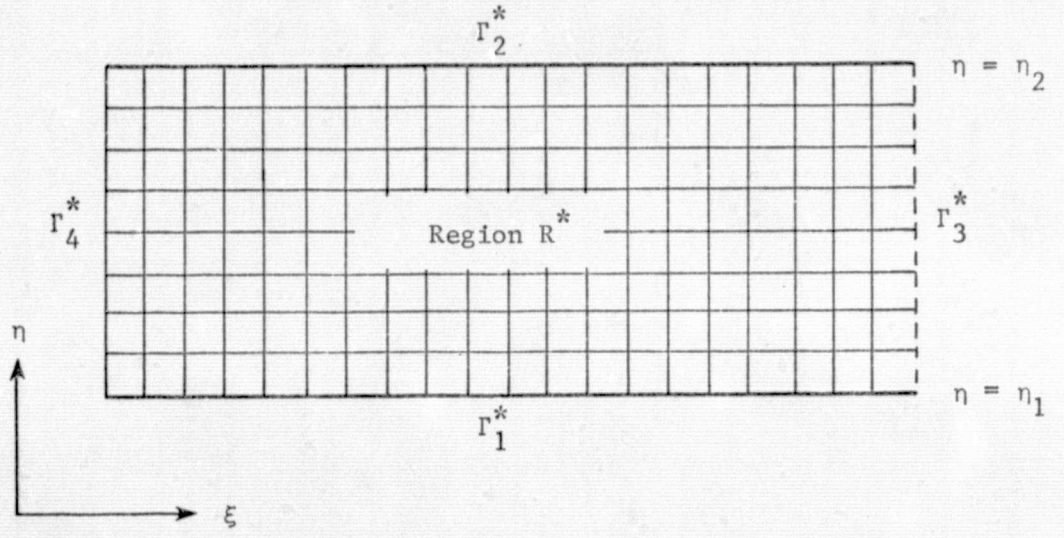

(b) Transformed Plane

Figure 1. Coordinate Transformation

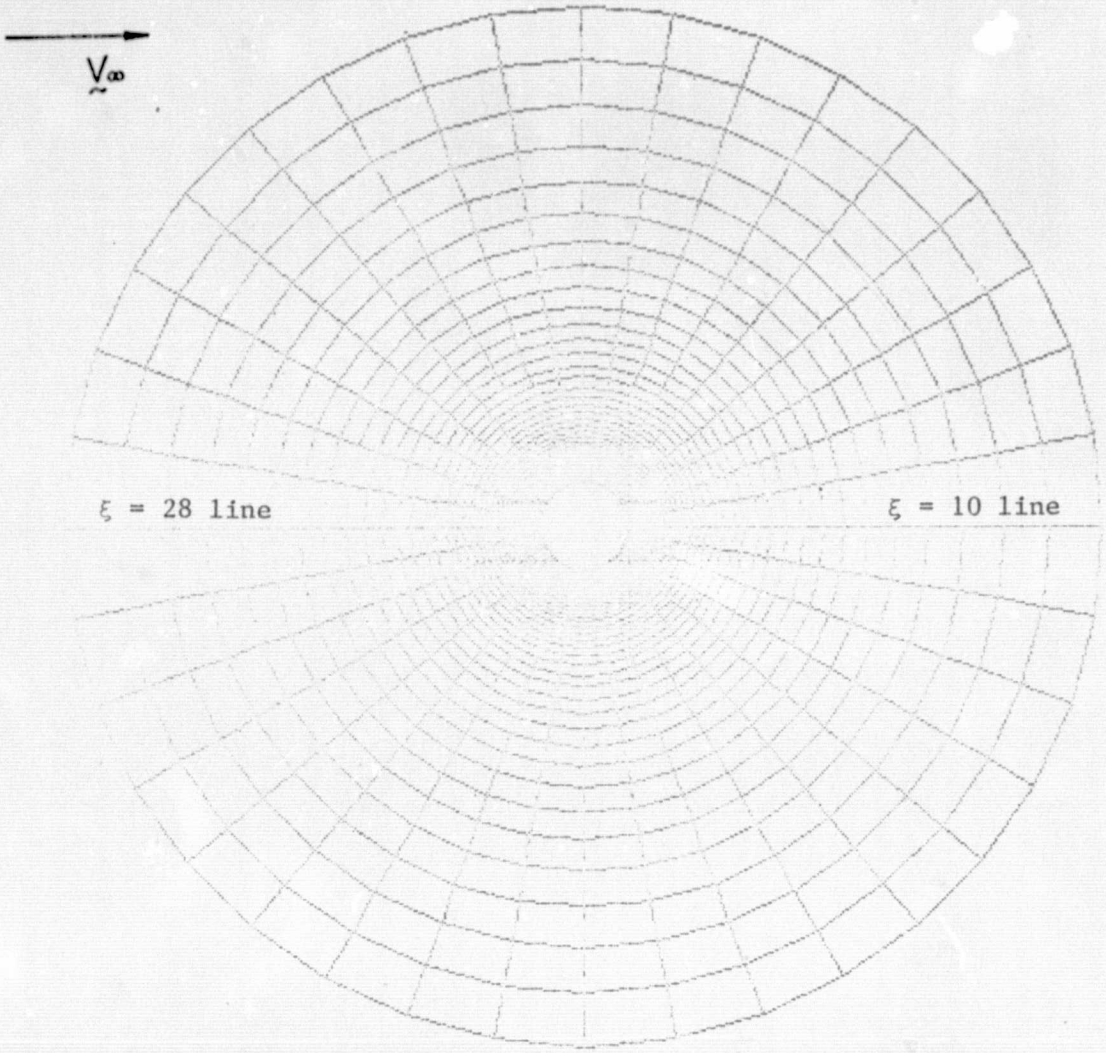

Figure 2. Coordinate System - 37 by 40 Field

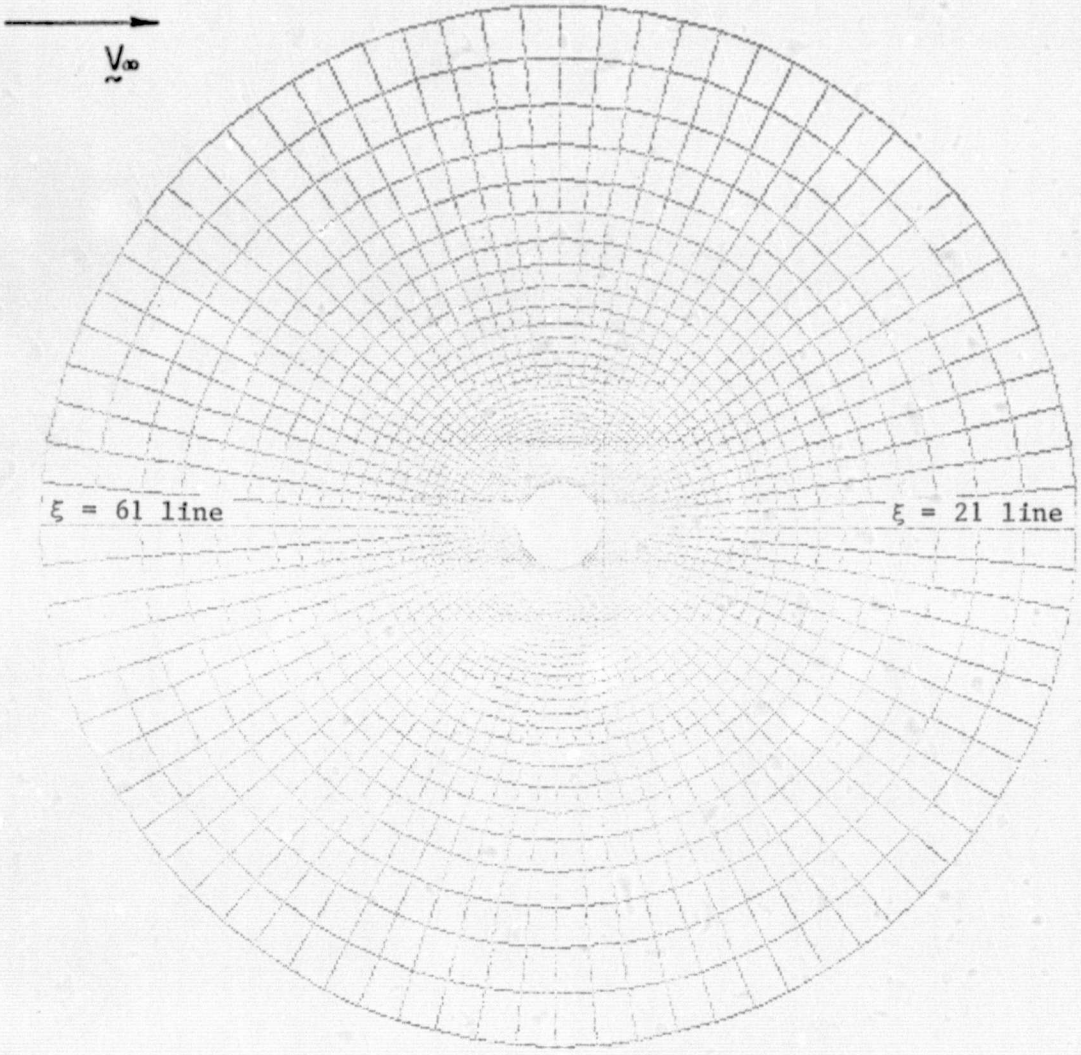

Figure 3. Coordinate System - 81 by 40 Field

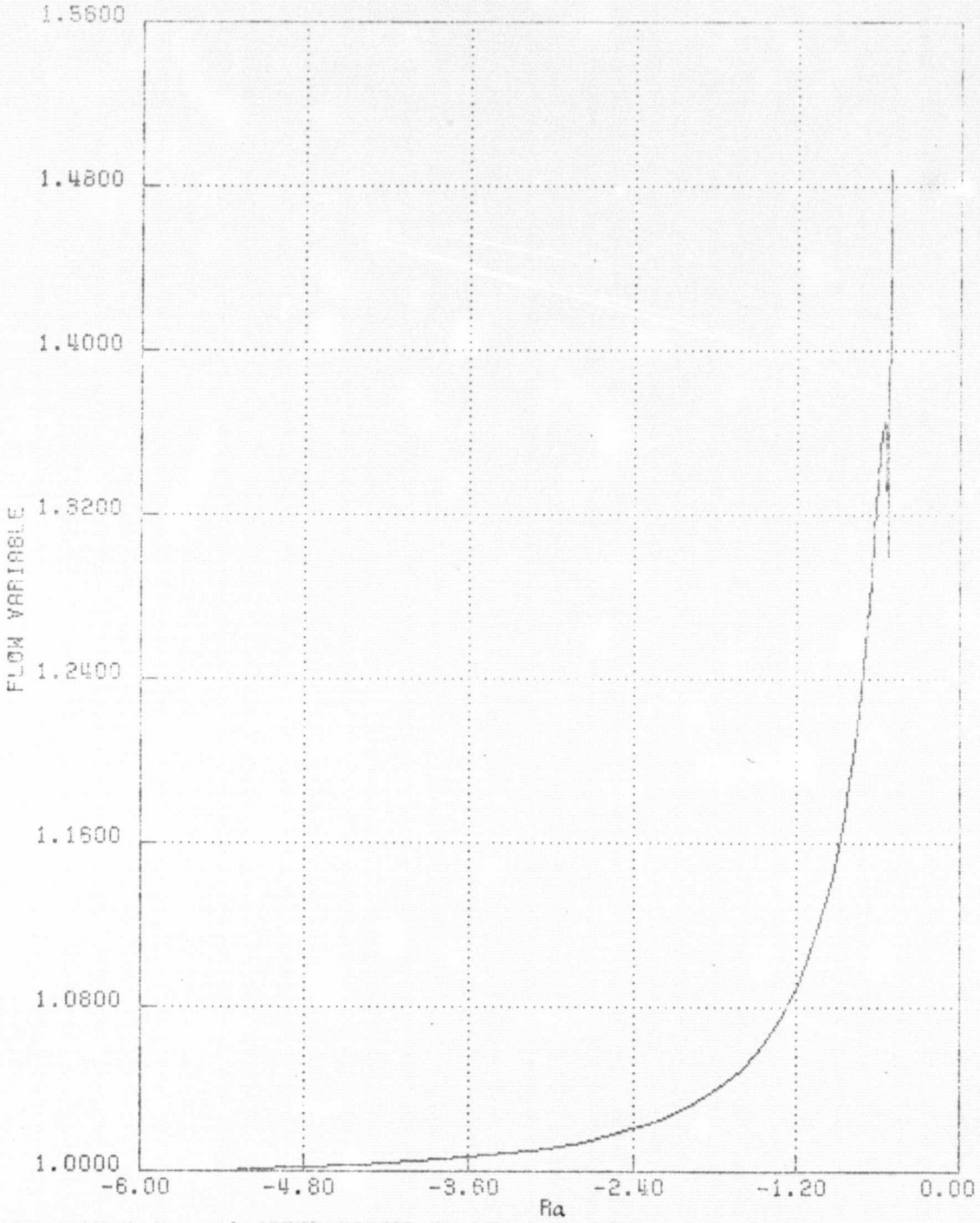

(a) Along ξ = 28 line

Figure 4a. Density Profile with New Formulation for Pressure Gradients at t = 0.1 (37 by 40 Field)

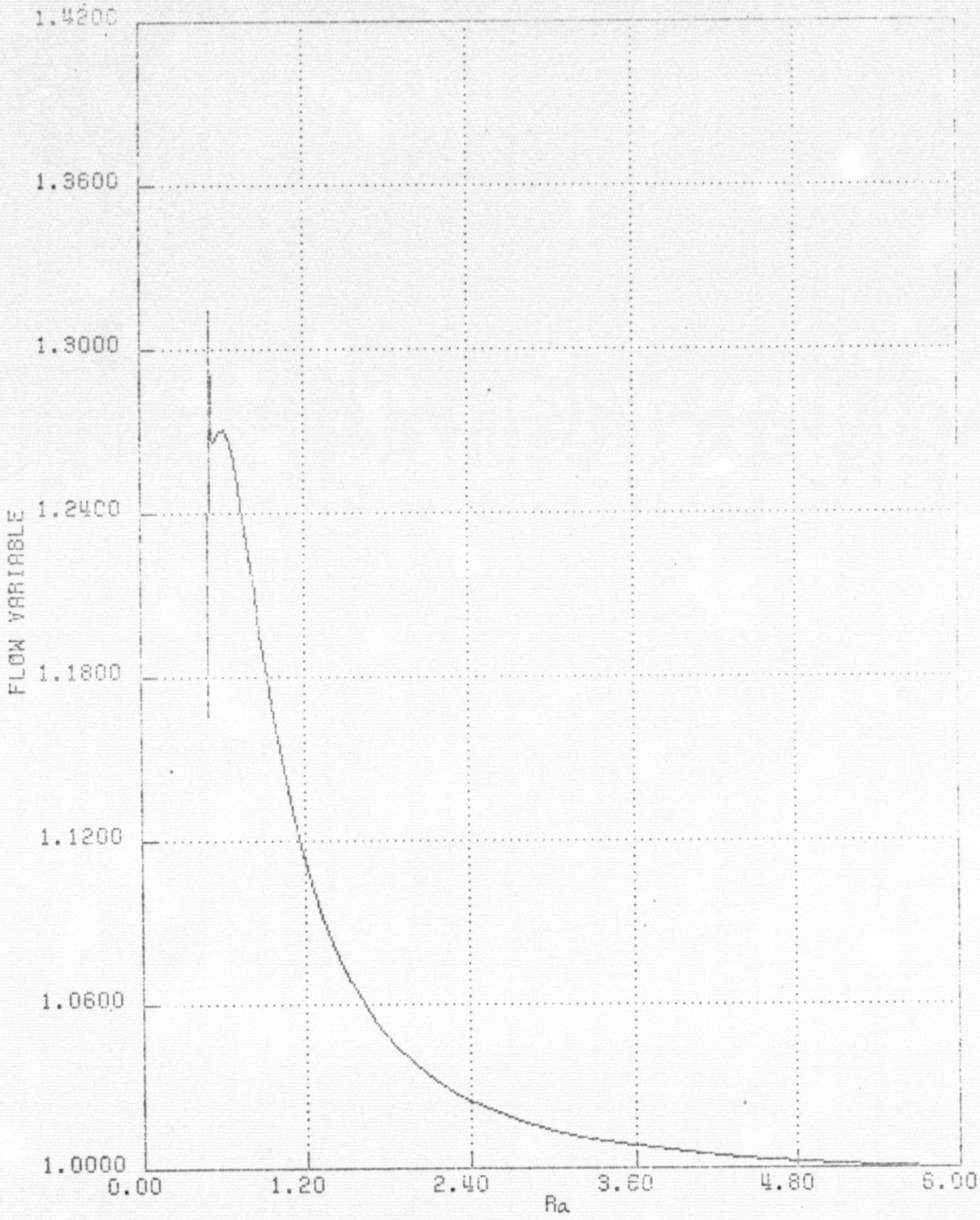

(b) Along ξ = 10 line

Figure 4b. Density Profile with New Formulation for Pressure Gradients at t = 0.1 (37 by 40 Field)

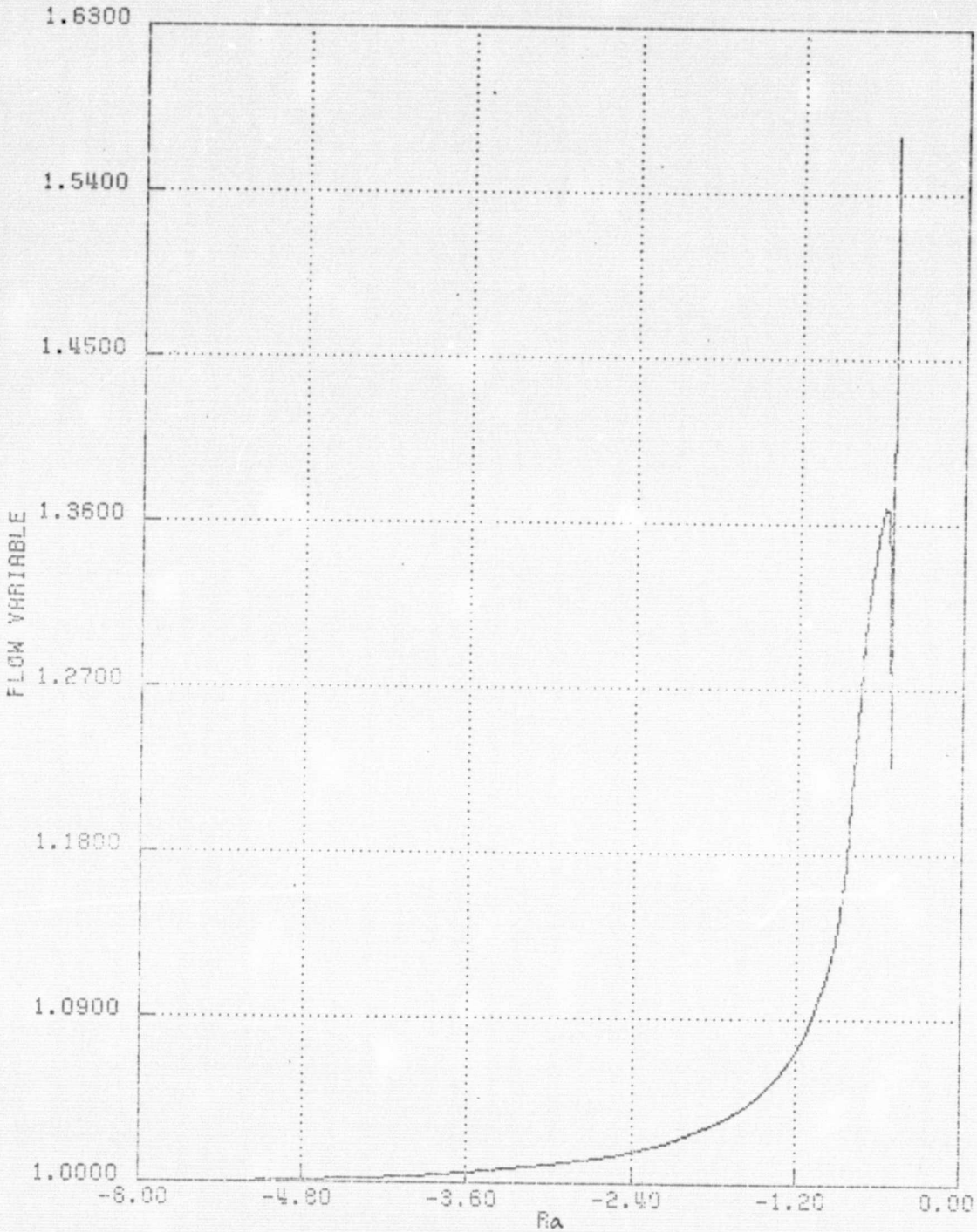

(a) Along ξ = 28 line

Figure 5a. Density Profile with New Formulation for Pressure Gradients at t = 0.3 (37 by 40 Field)

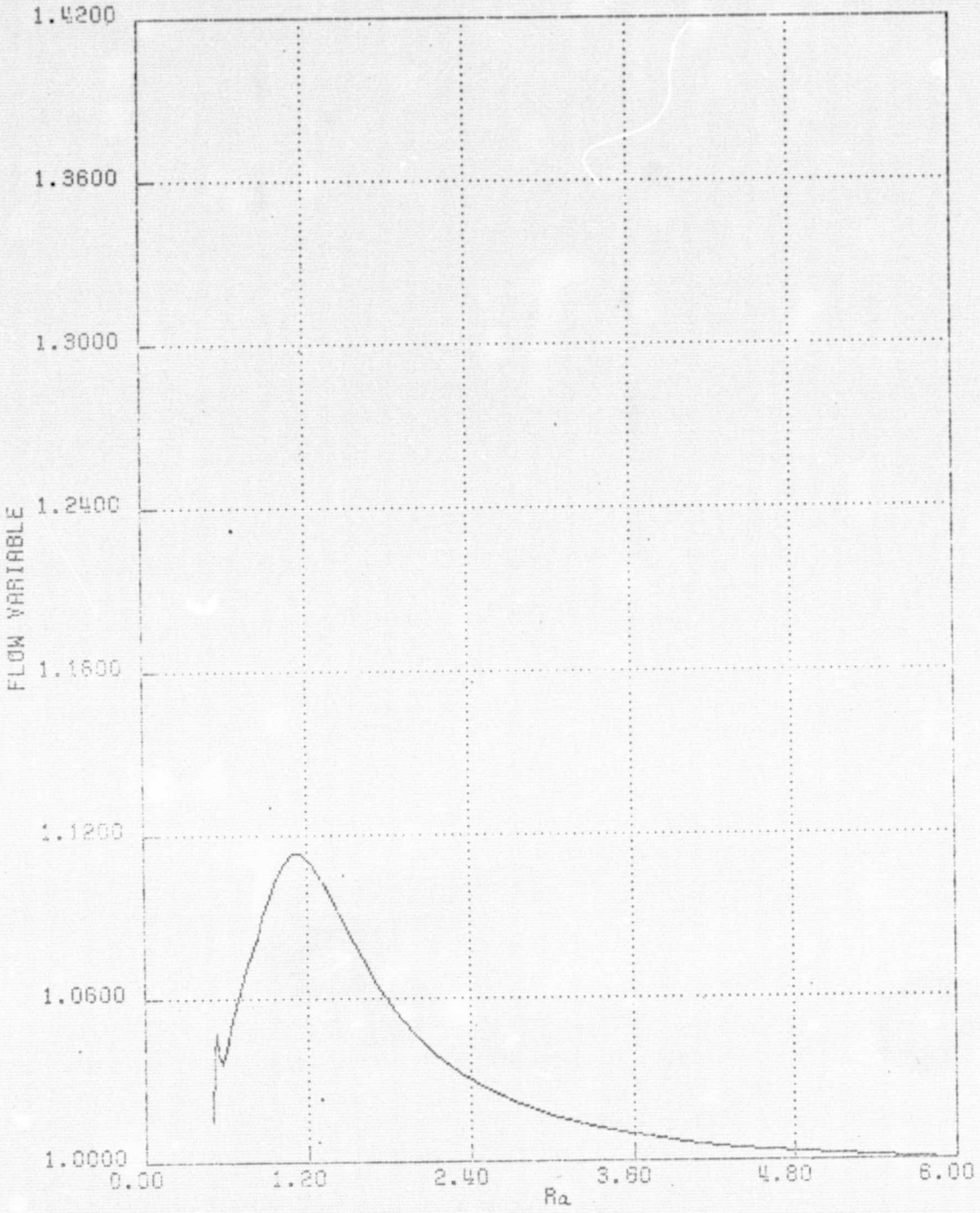

(b) Along ξ = 10 line

Figure 5b. Density Profile with New Formulation for Pressure Gradients at t = 0.3 (37 by 40 Field)

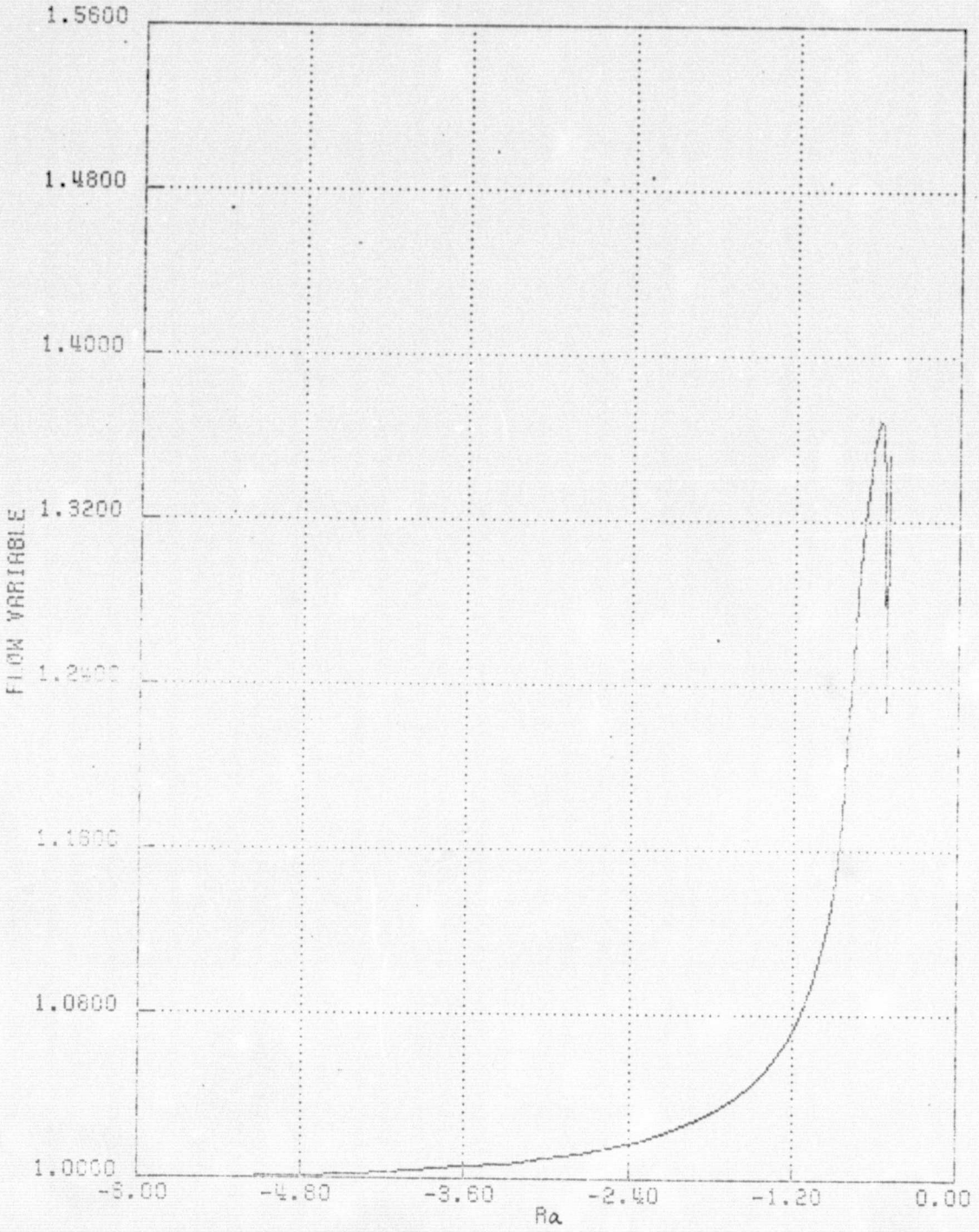

(a) Along ξ = 28 line

Figure 6a. Density Profile with New Formulation for Body Density at t = 0.3 (37 by 40 Field)

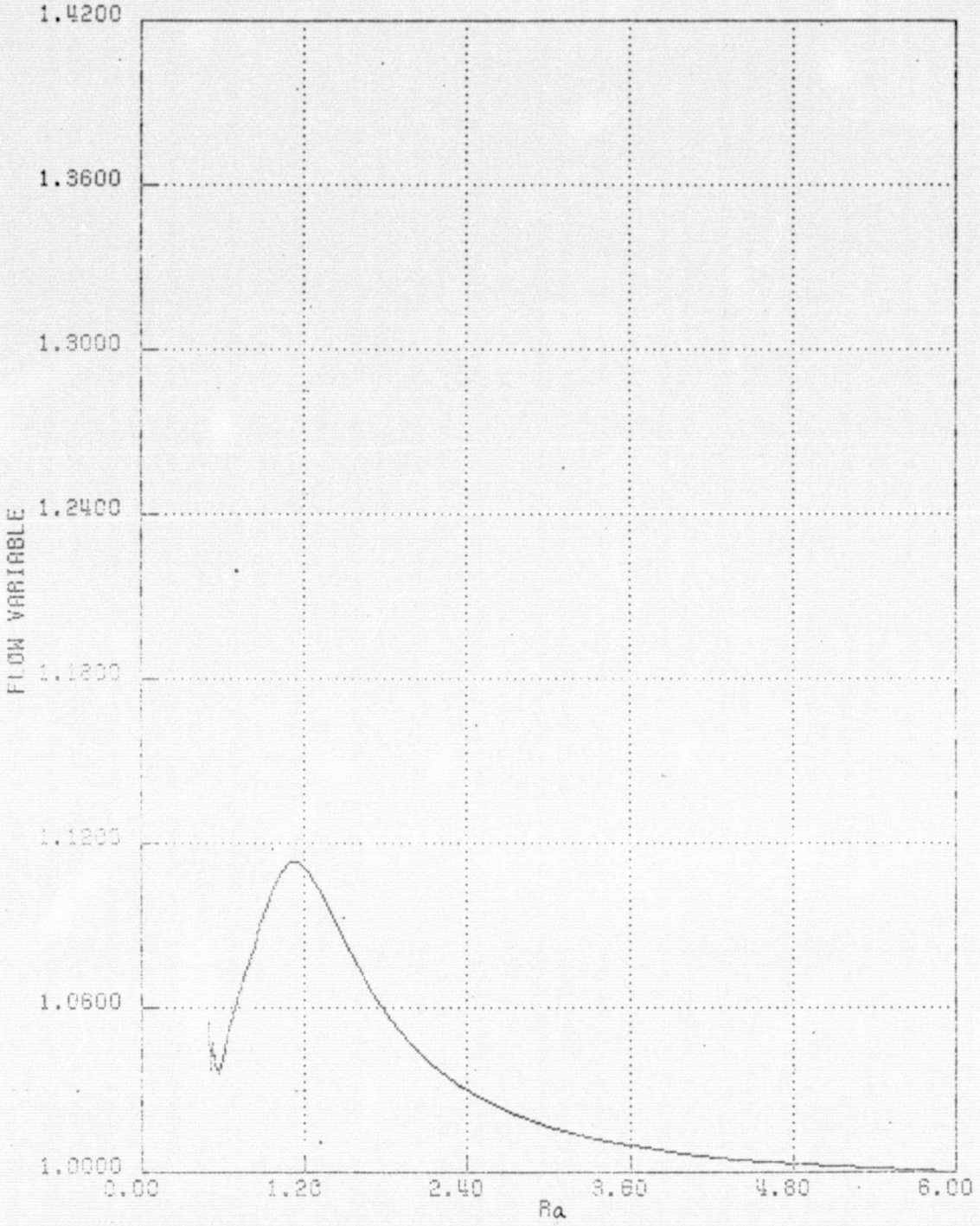

(b) Along ξ = 10 line

Figure 6b. Density Profile with New Formulation for Body Density at t = 0.3 (37 by 40 Field)

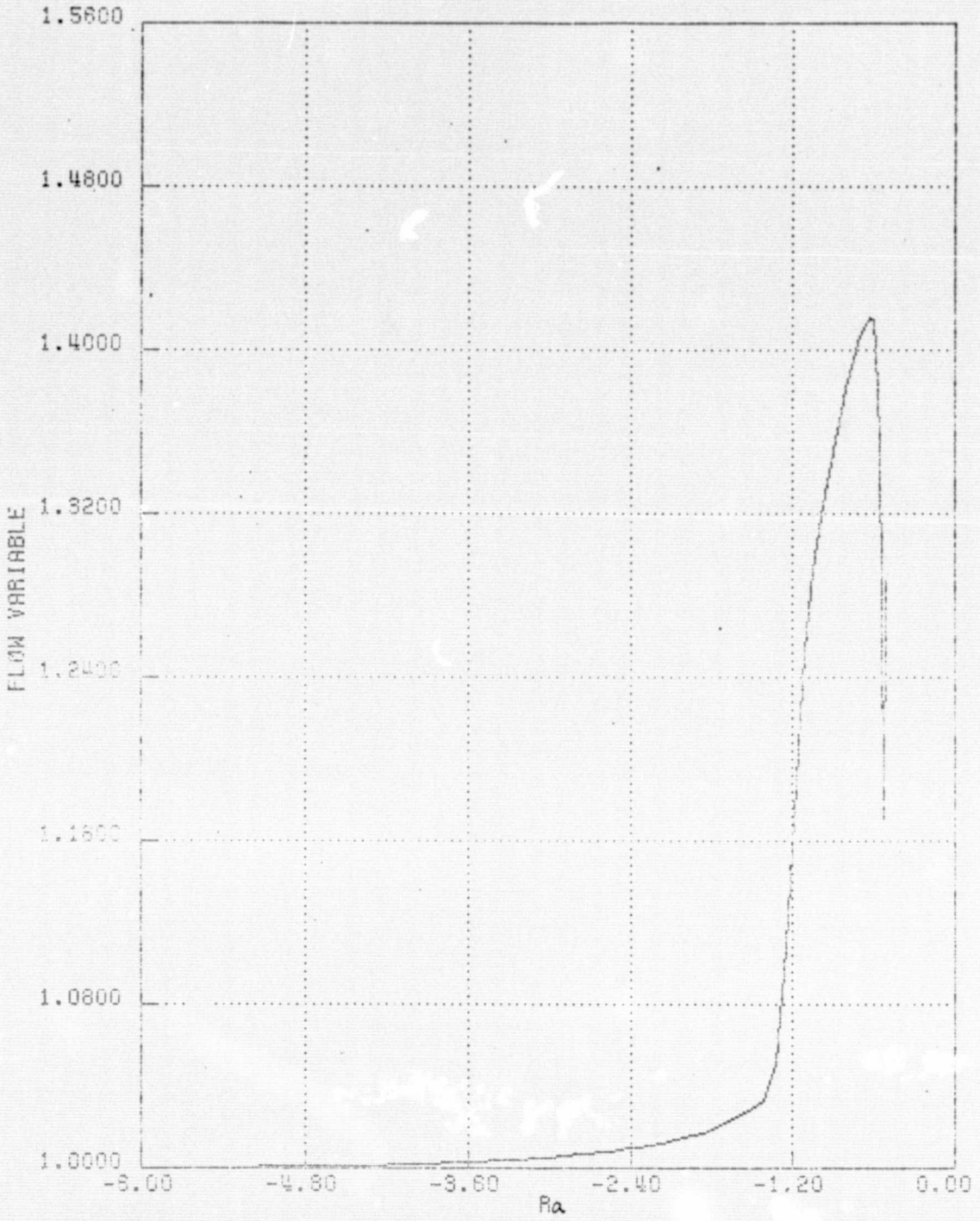

(a) Along ξ = 28 line

Figure 7a. Density Profile with New Formulation for Body Density at t = 1.0 (37 by 40 Field)

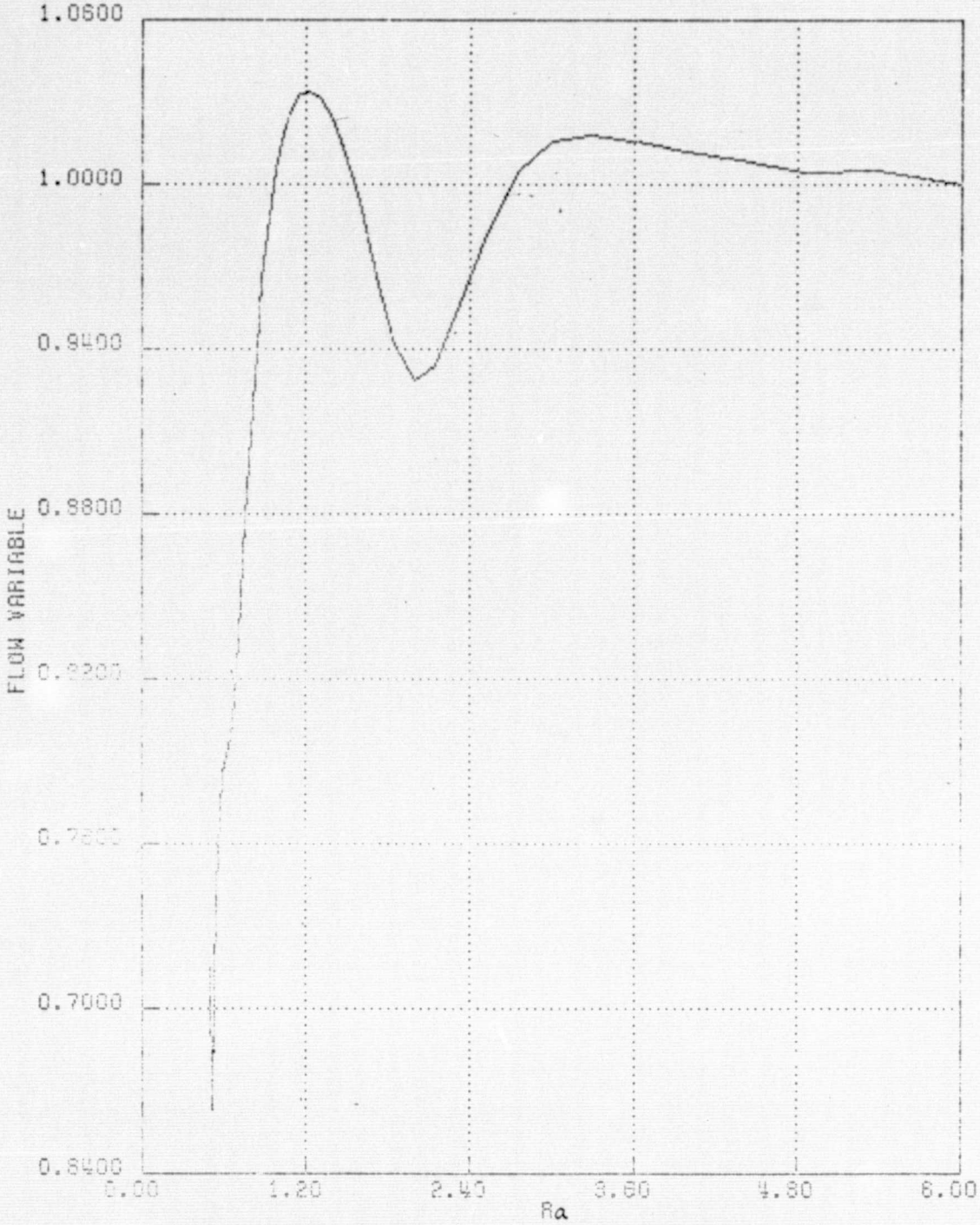

(b) Along ξ = 10 line

Figure 7b. Density Profile with New Formulation for Body Density at t = 1.0 (37 by 40 Field)

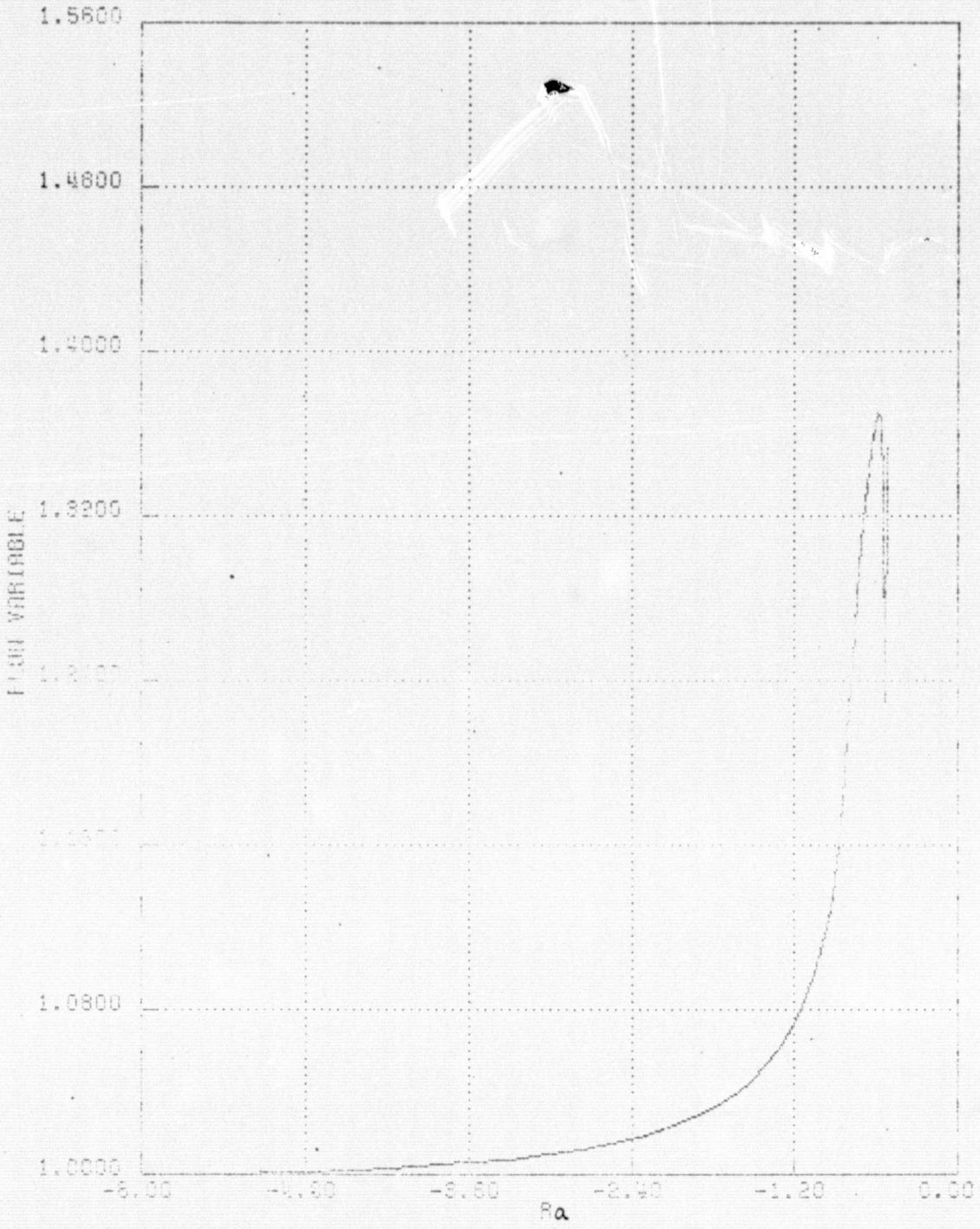

(a) Along ξ = 28 line

Figure 8a. Density Profile with Δt = 0.02 at t = 0.3 (37 by 40 Field)

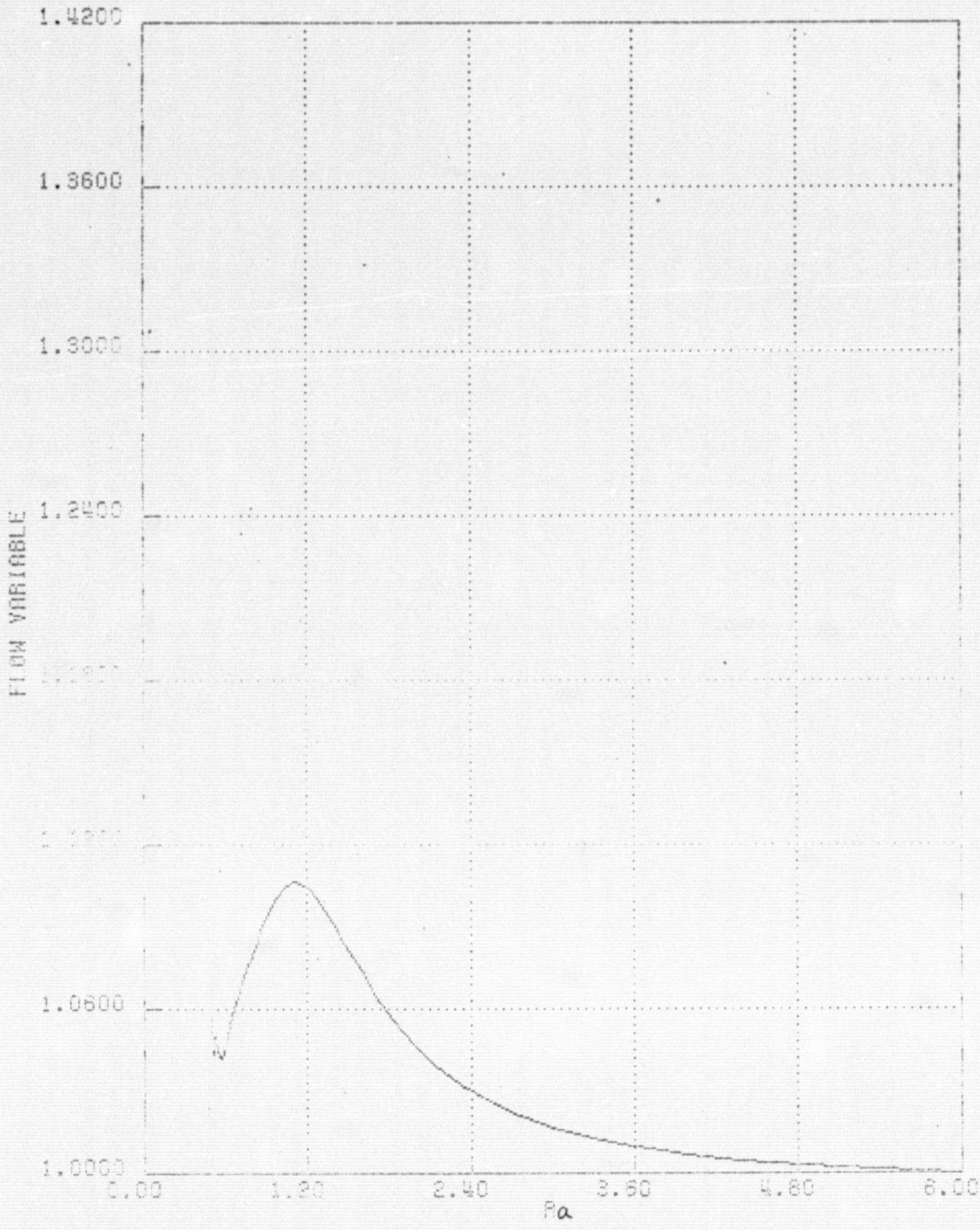

(b) Along ξ = 10 line

Figure 8b. Density Profile with $\Delta t = 0.02$ at $t = 0.3$ (37 by 40 Field)

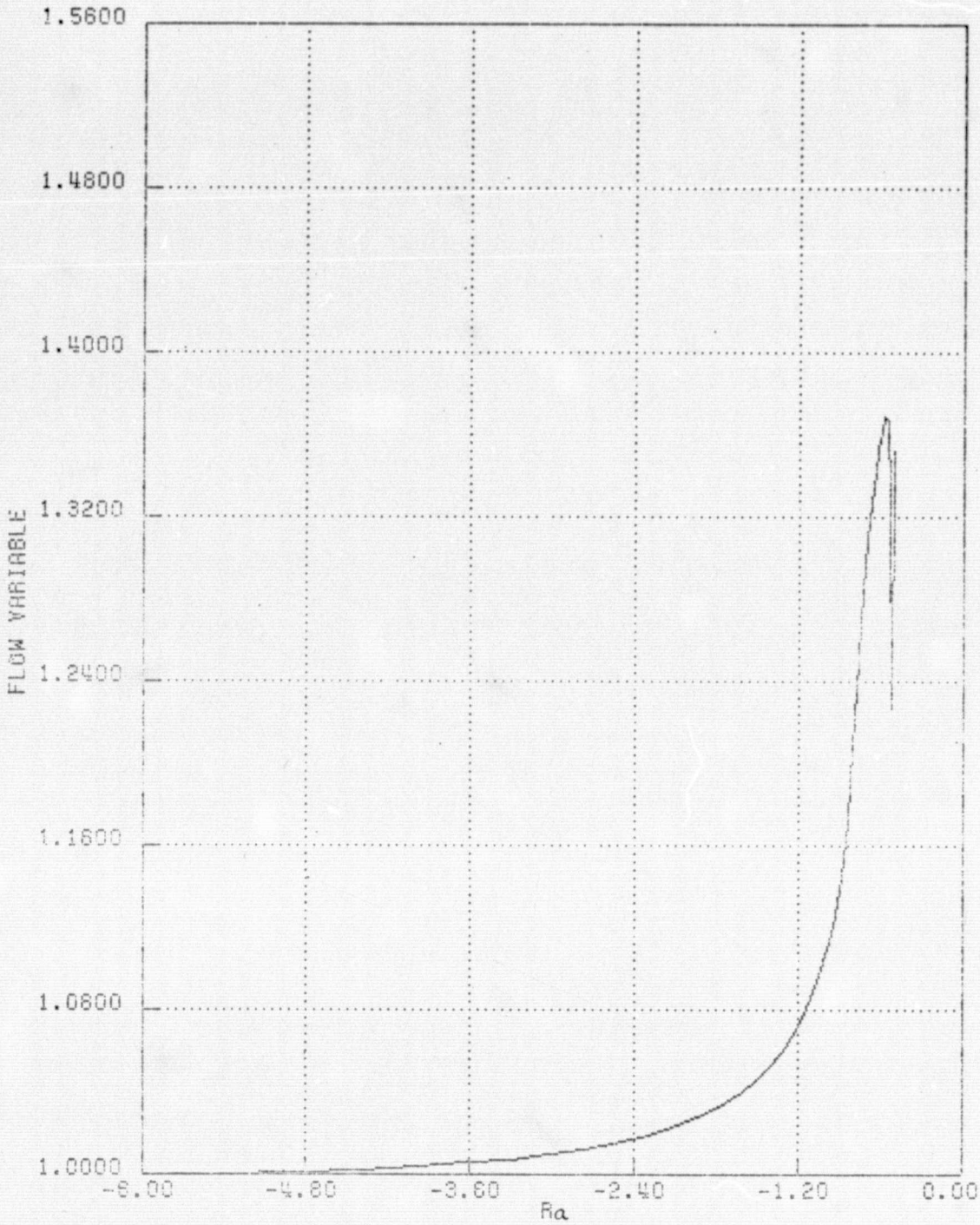

(a) Along ξ = 28 line

Figure 9a. Density Profile with $\Delta t = 0.005$ at $t = 0.3$ (37 by 40 Field)

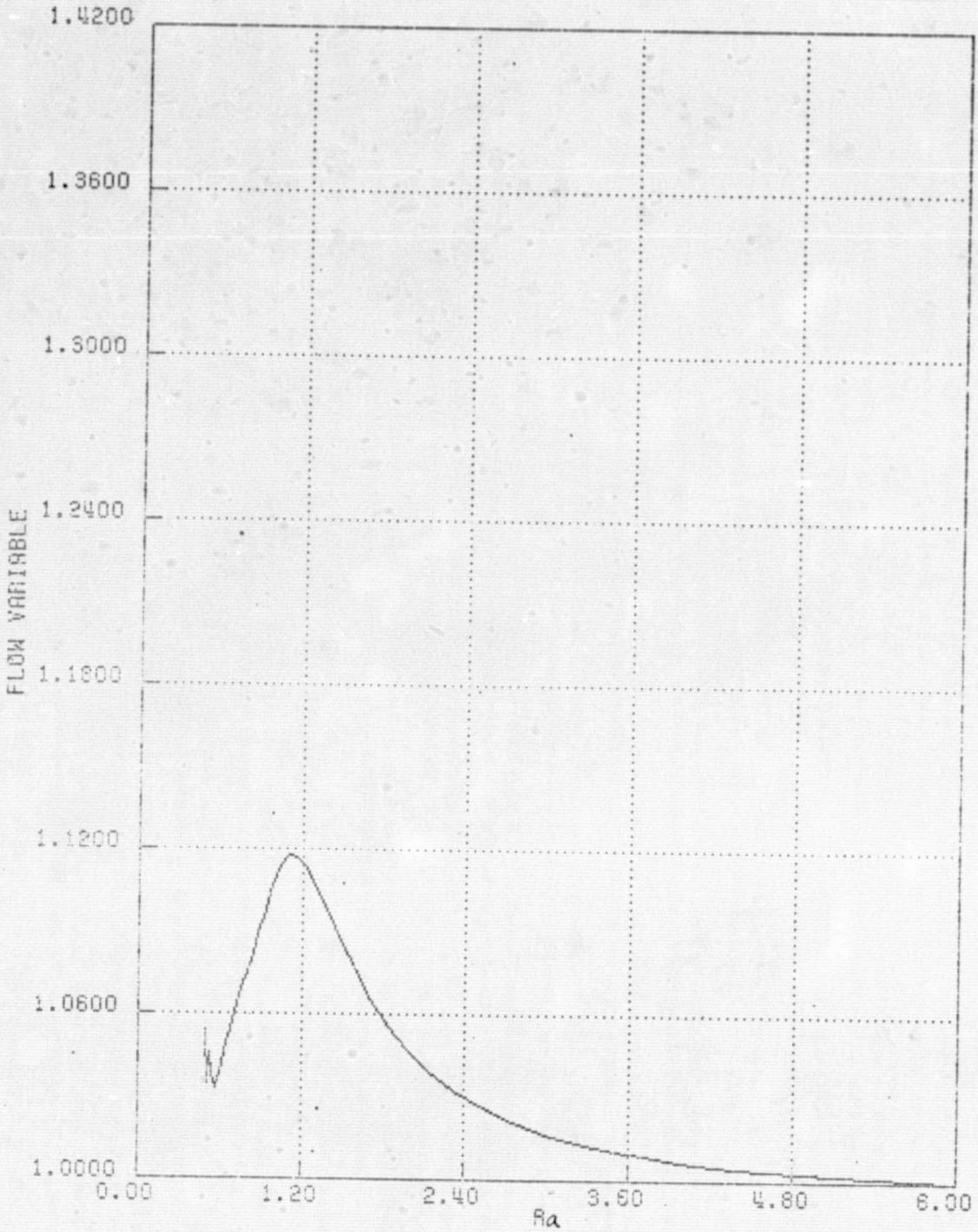

(b) Along ξ = 10 line

Figure 9b. Density Profile with Δt = 0.005 at t = 0.3 (37 by 40 Field)

(a) Along ξ = 28 line

Figure 10a. Density Profile with t = 0.005 at t = 1.0 (37 by 40 Field)

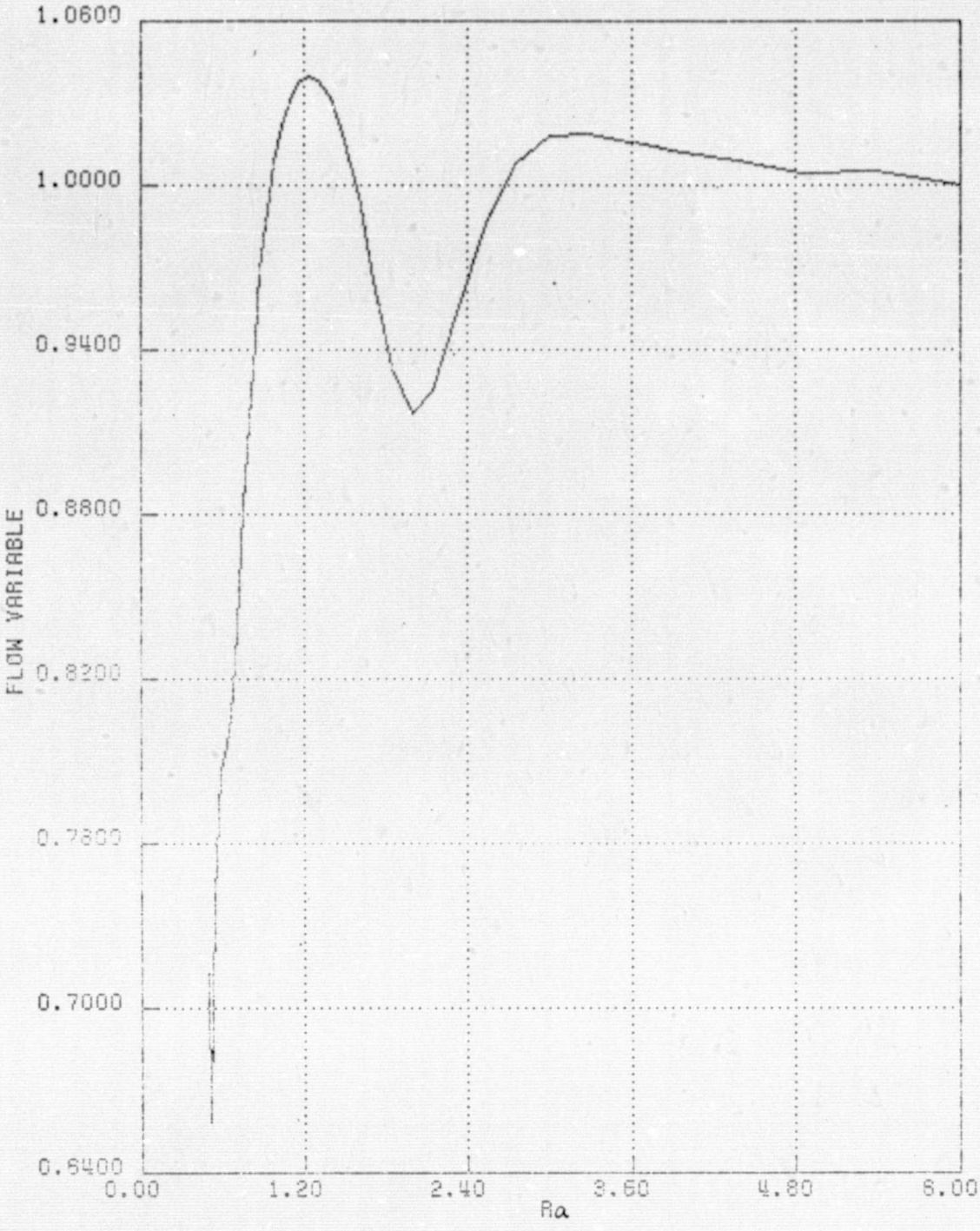

(b) Along ξ = 10 line

Figure 10b. Density Profile with t = 0.005 at t = 1.0 (37 by 40 Field)

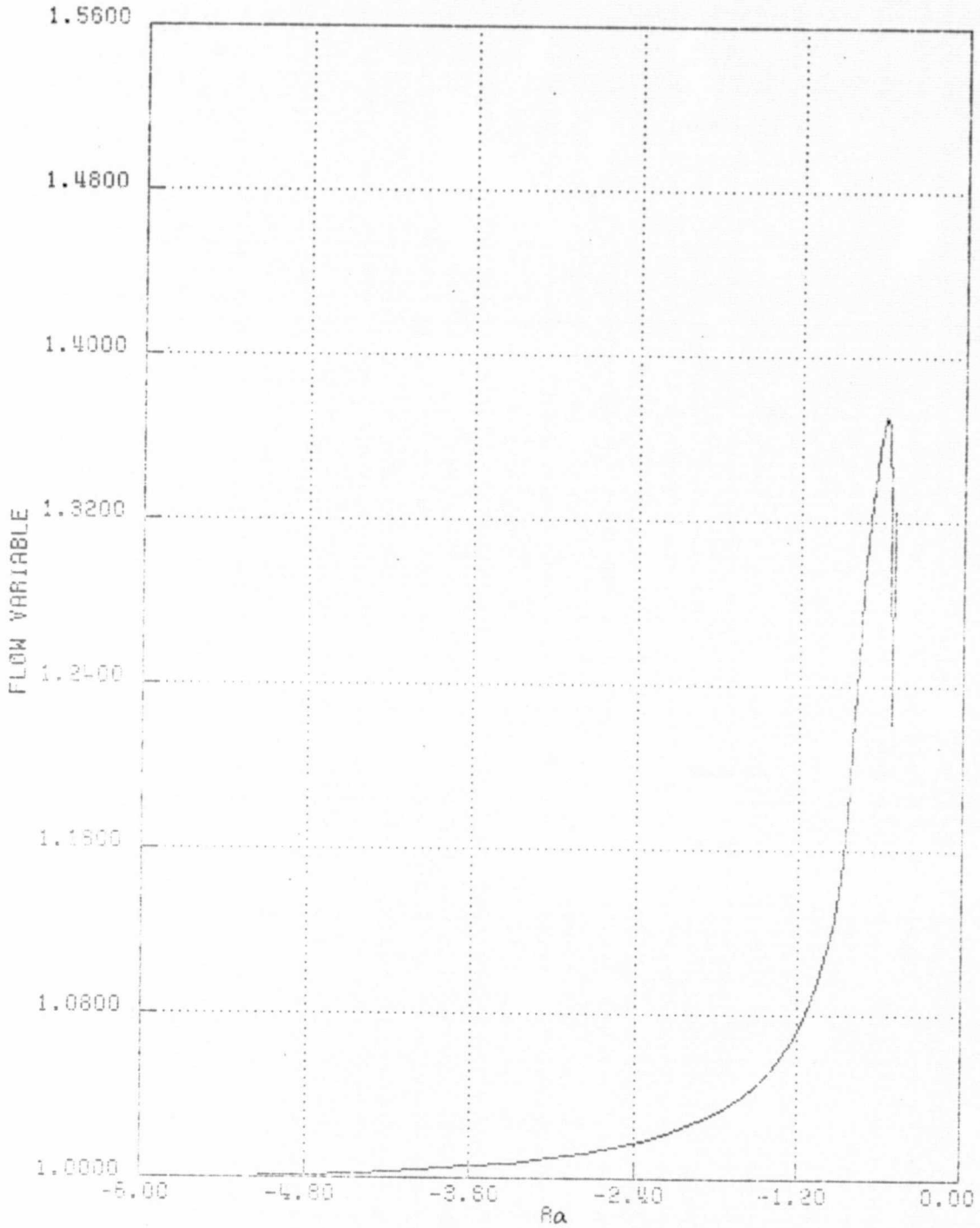

(a) Along ξ = 28 line

Figure 11a. Density Profile with A Constant Temperature Wall at t = 0.3 (37 by 40 Field)

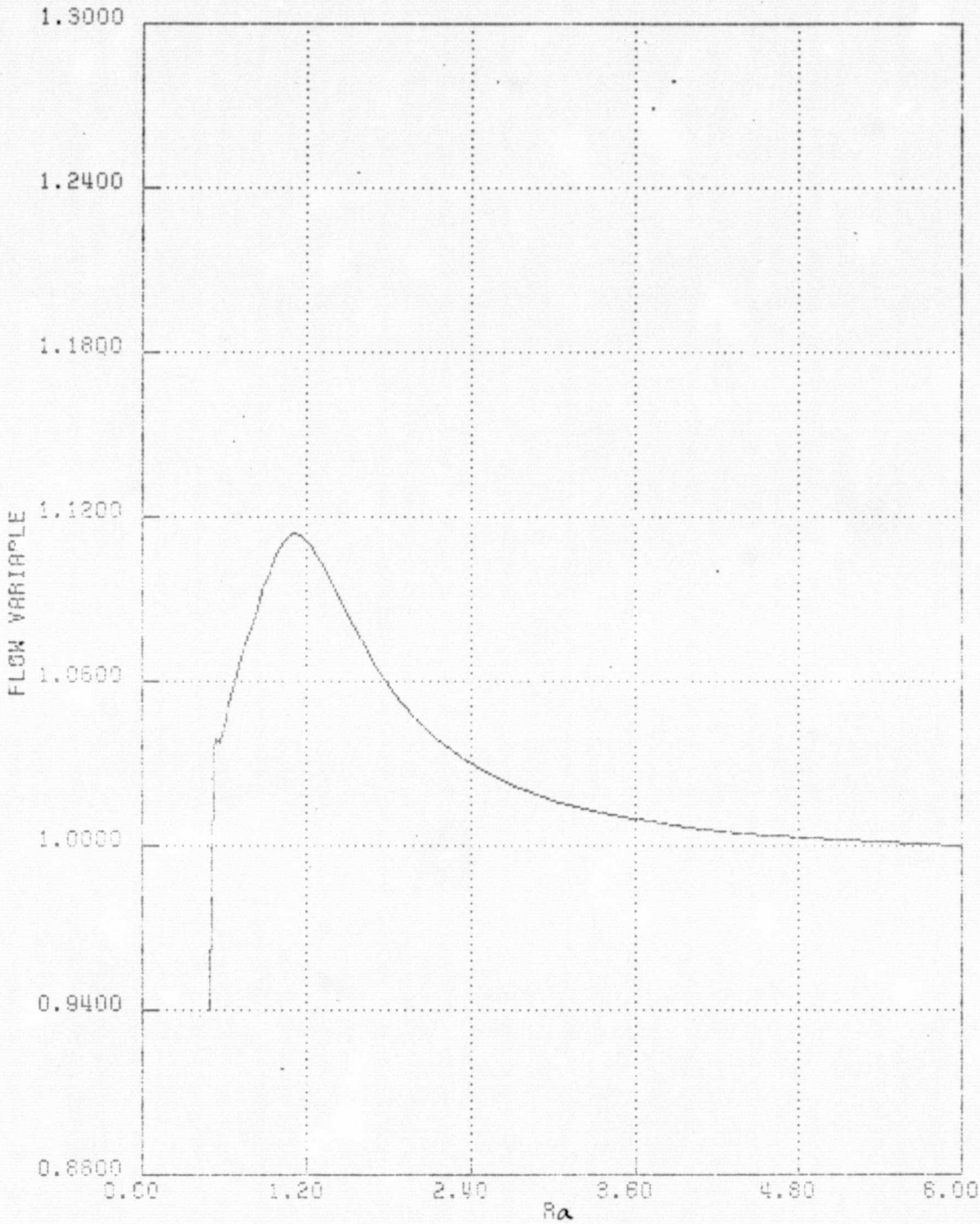

(b) Along ξ = 10 line

Figure 11b. Density Profile with A Constant Temperature Wall at t = 0.3 (37 by 40 Field)

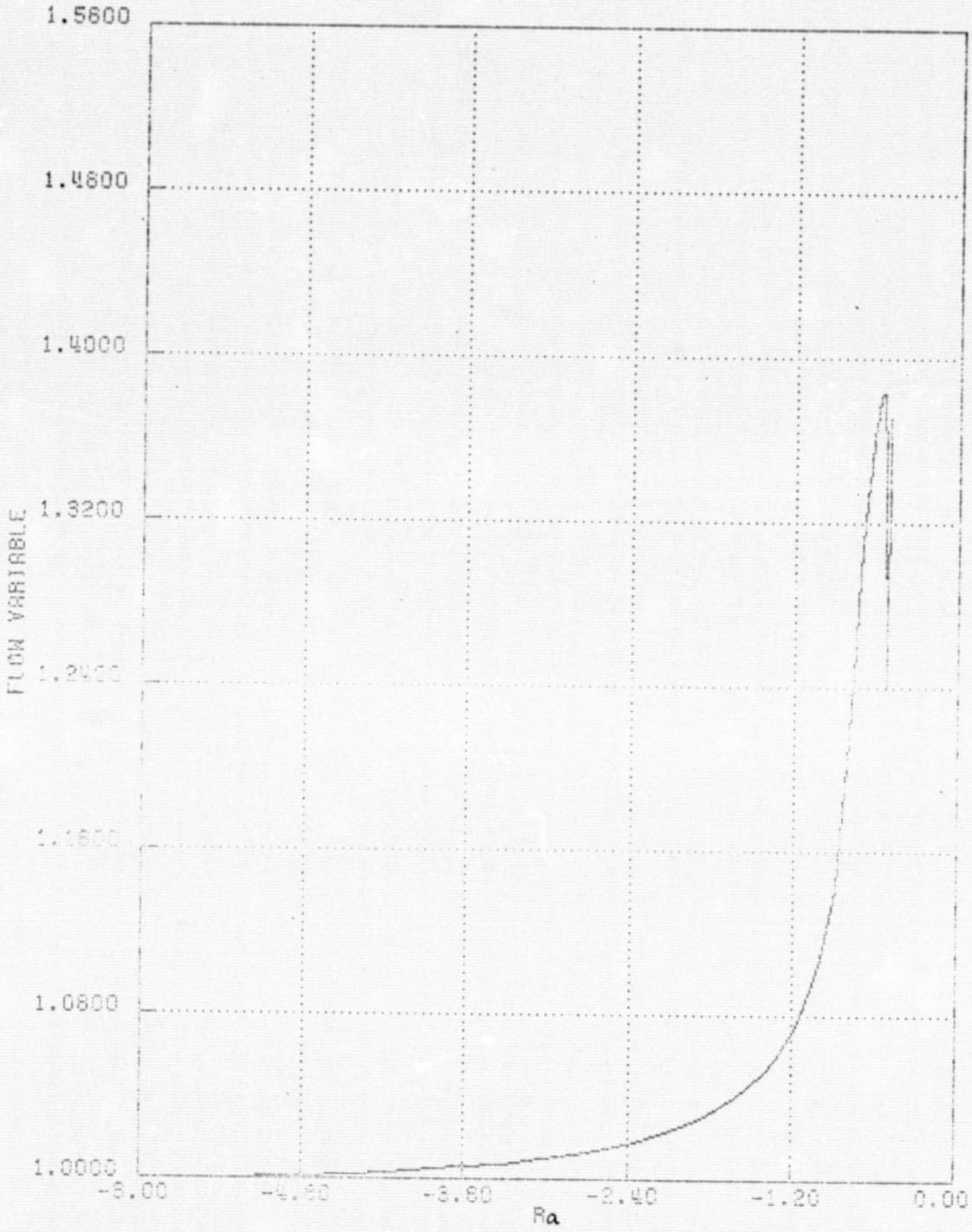

(a) Along ξ = 61 line

Figure 12a. Density Profile with New Formulations at t = 0.3 (81 by 40 Field)

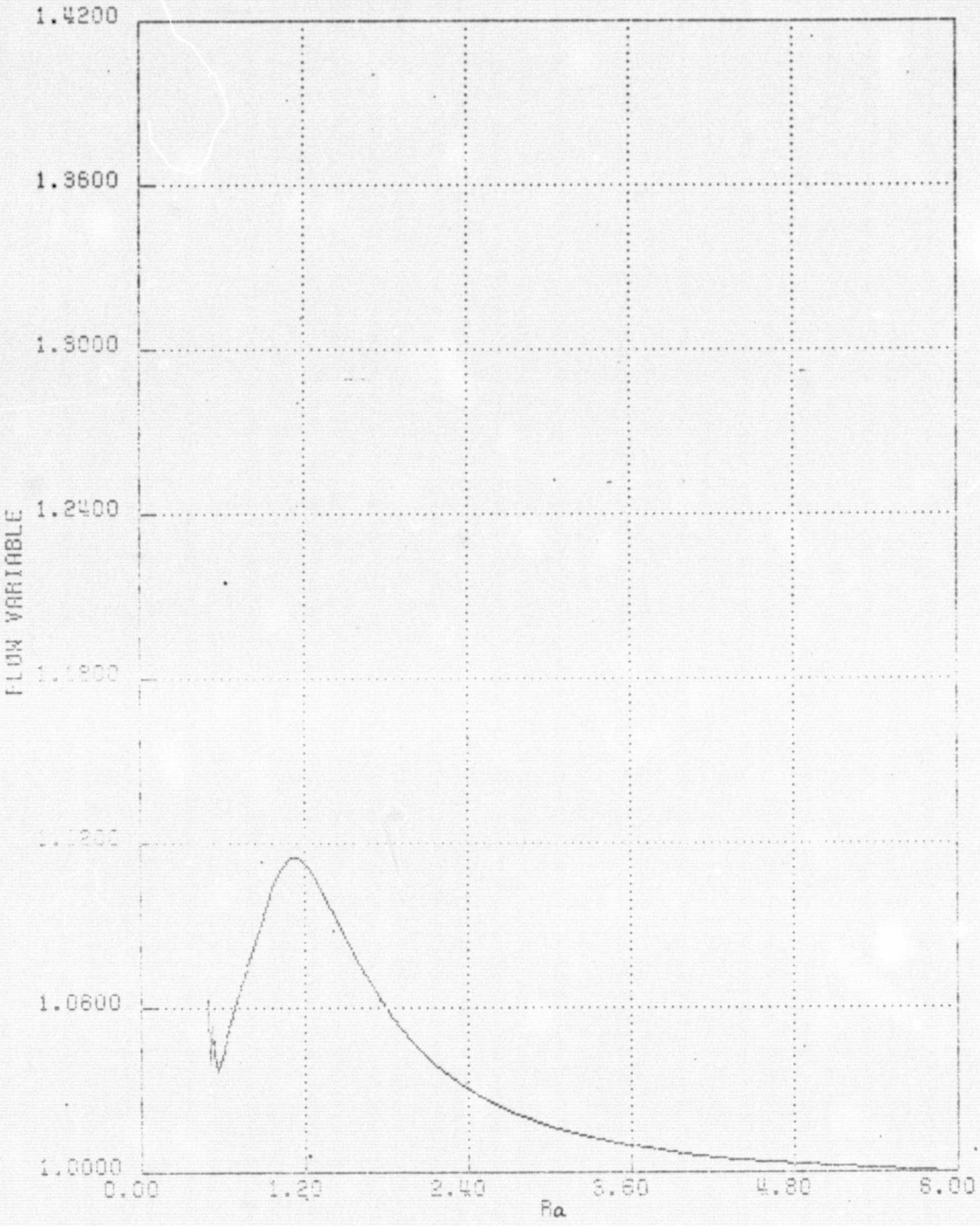

(b) Along ξ = 21 line

Figure 12b. Density Profile with New Formulations at t = 0.3 (81 by 40 Field)

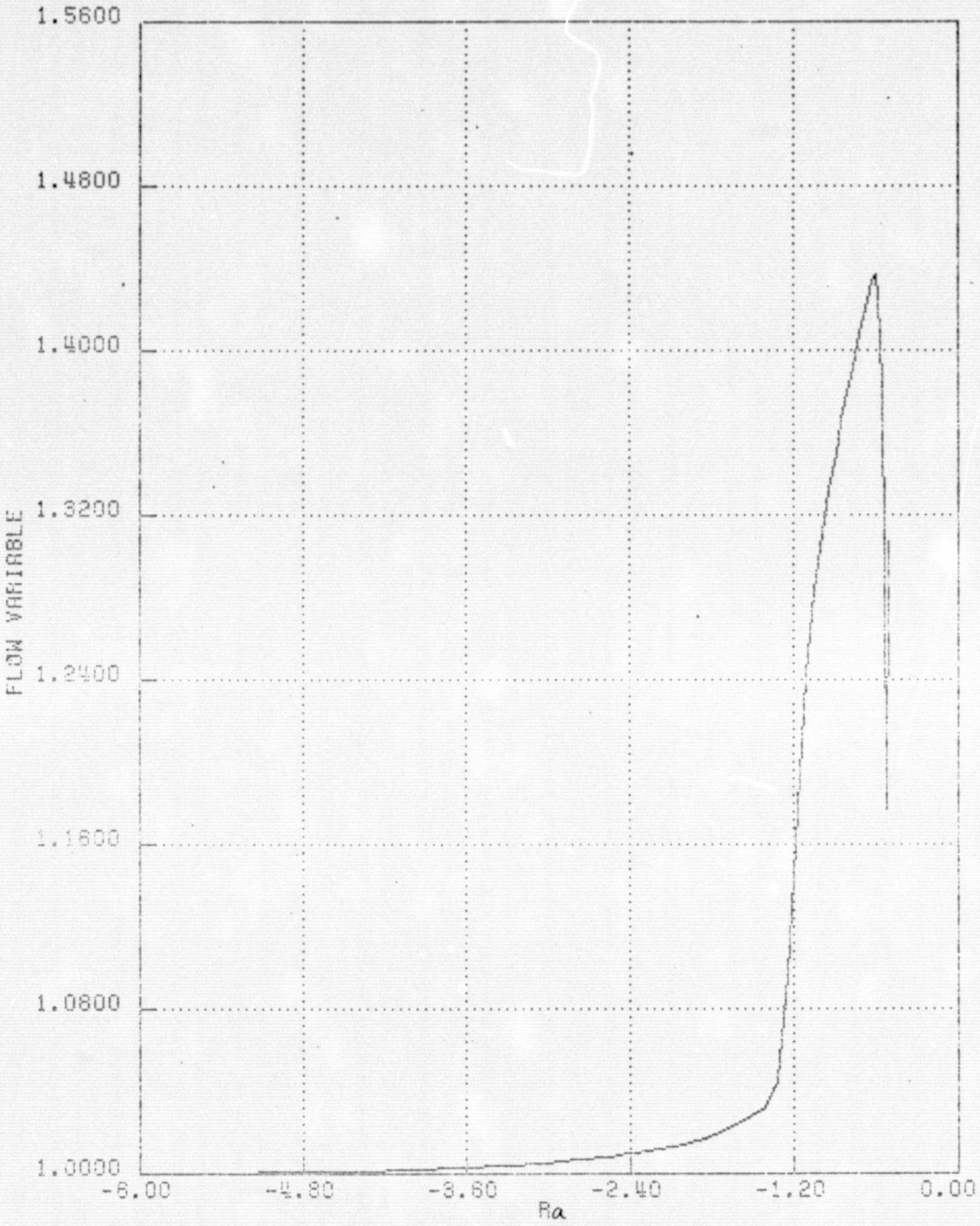

(a) Along ξ = 61 line

Figure 13a. Density Profile with New Formulations at t = 1.0 (81 by 40 Field)

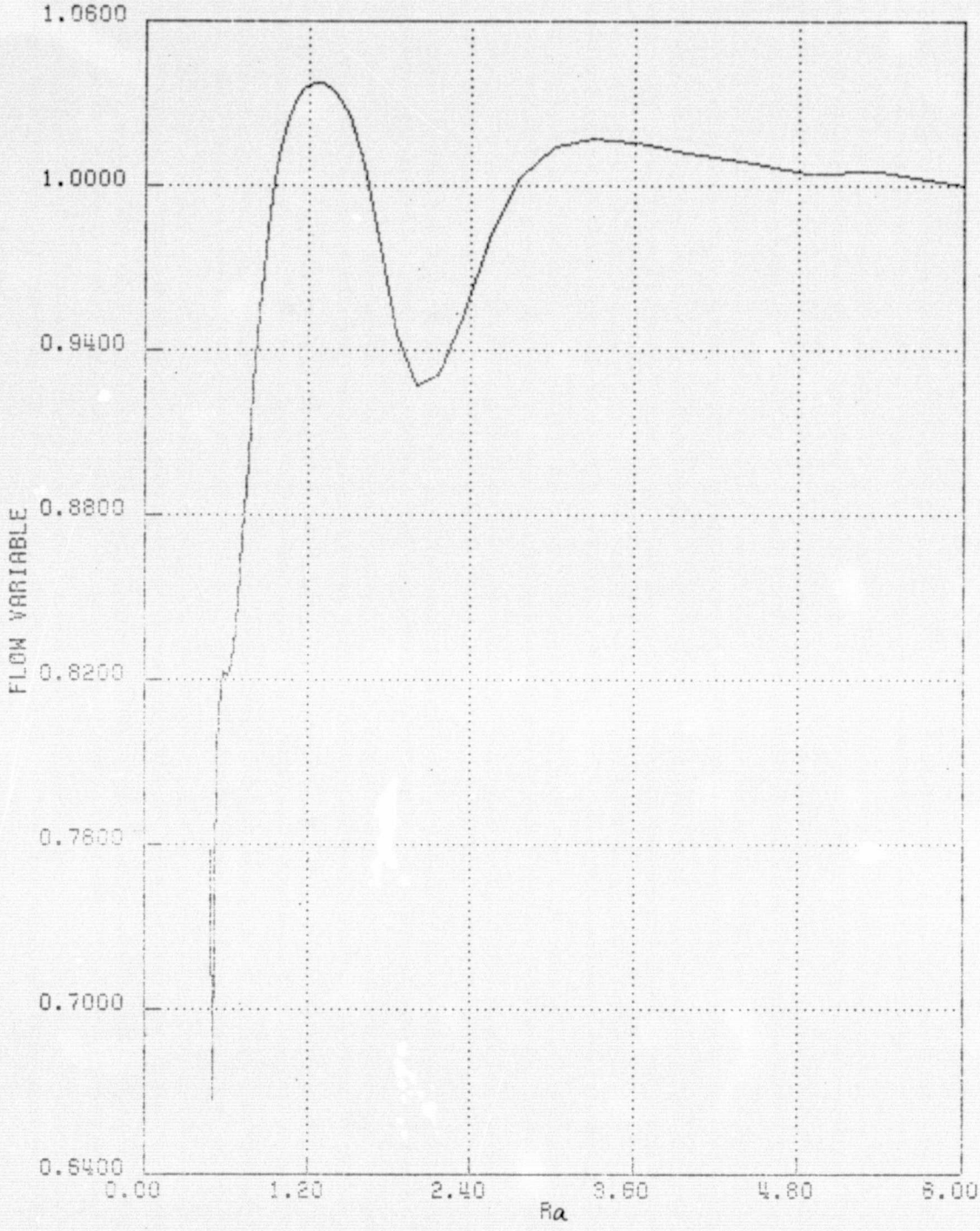

(b) Along ξ = 21 line

Figure 13b. Density Profile with New Formulations at t = 1.0 (81 by 40 Field)

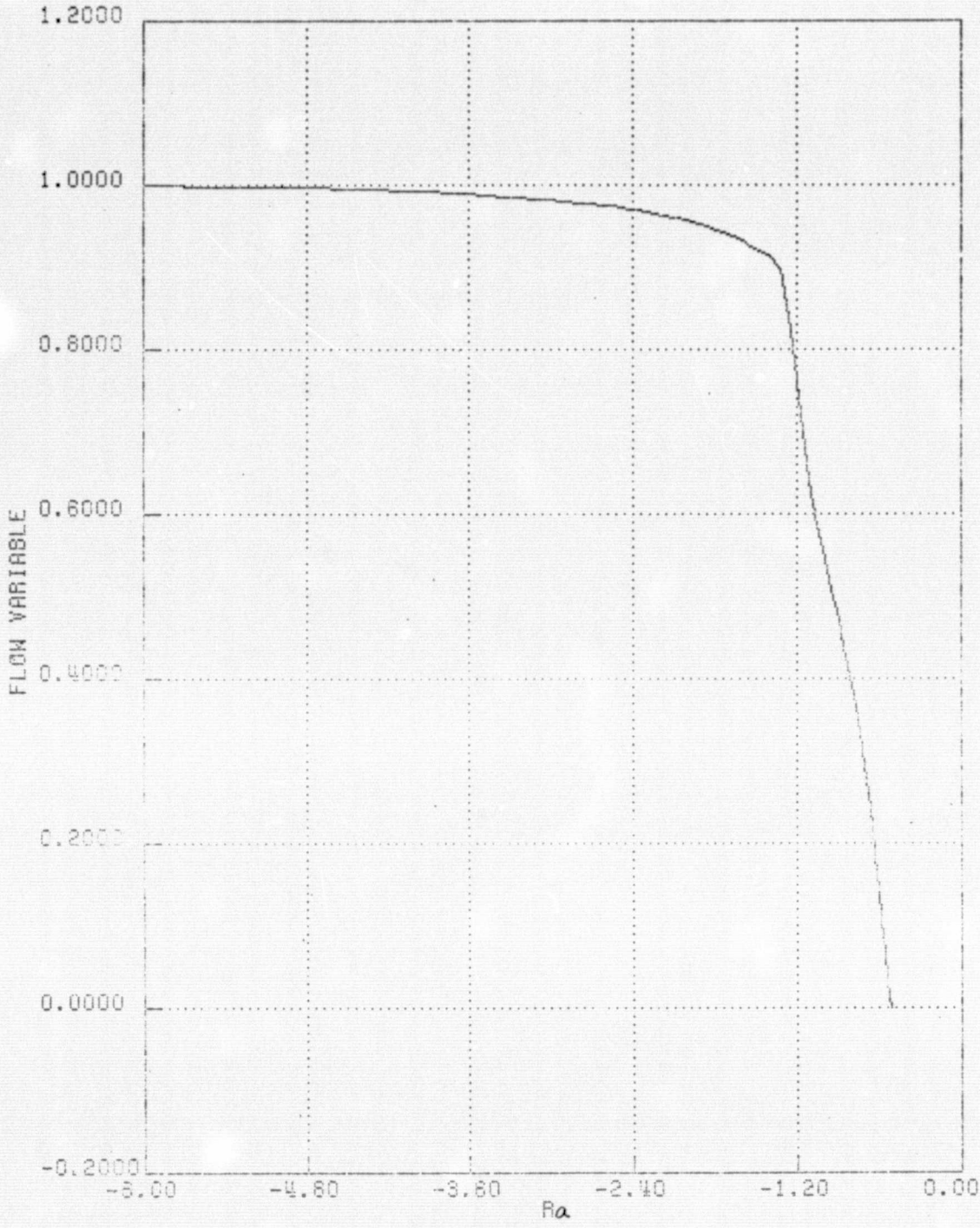

(a) Along ξ = 61 line

Figure 14a. Velocity Profile with New Formulations at t = 1.0 (81 by 40 Field)

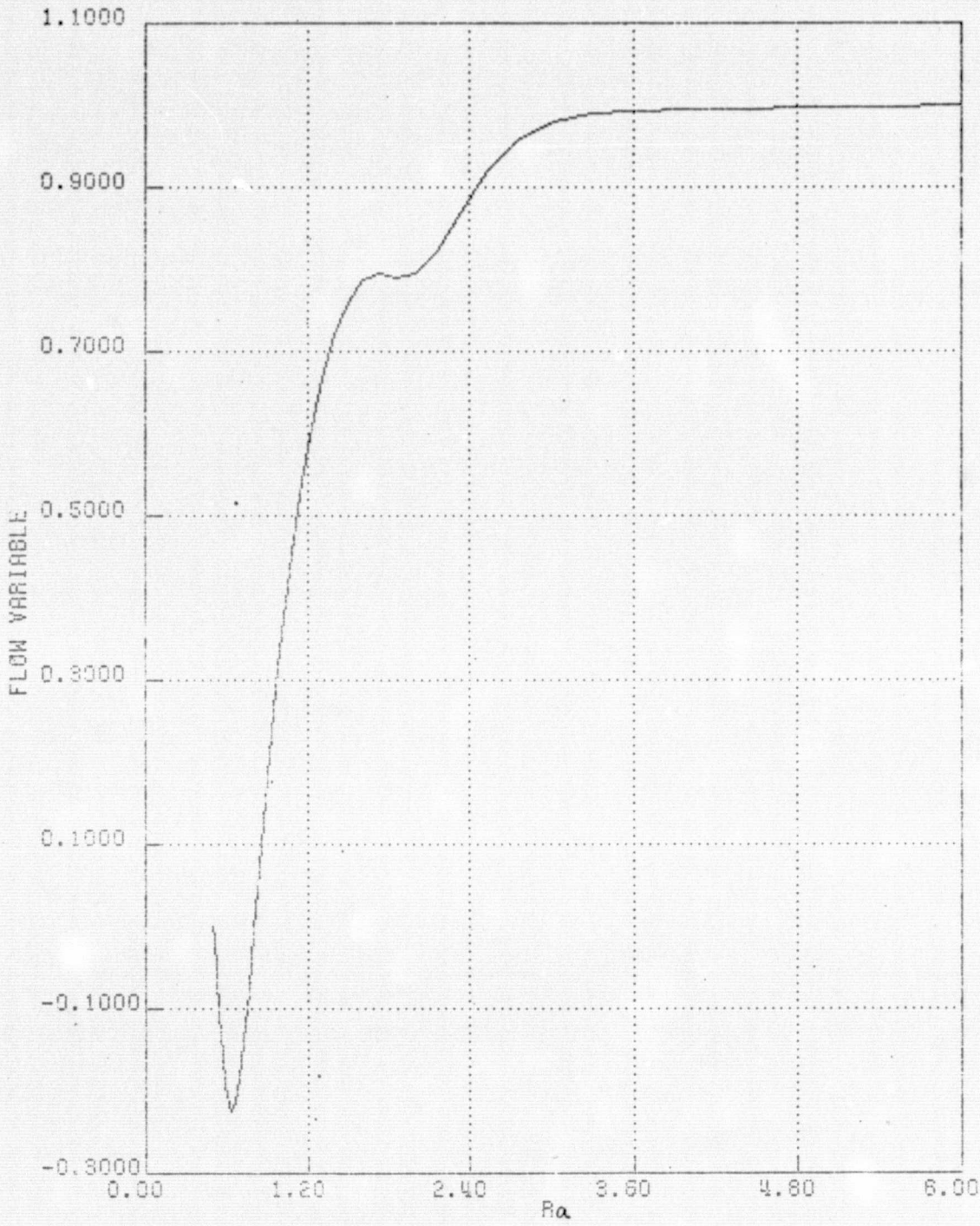

(b) Along ξ = 21 line

Figure 14b. Velocity Profile with New Formulations at t = 1.0 (81 by 40 Field)

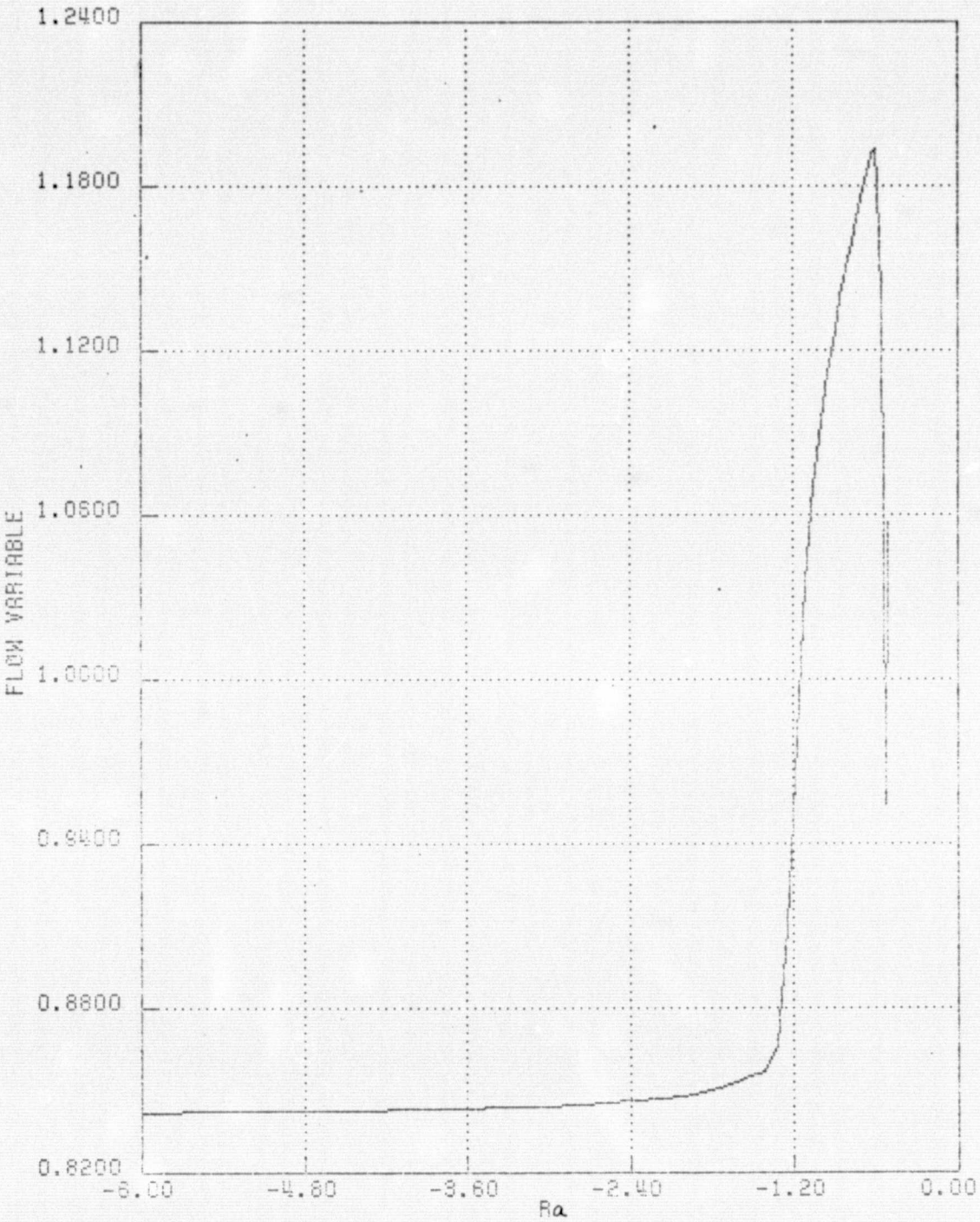

(a) Along ξ = 61 line

Figure 15a. Total Energy Profile with New Formulations at t = 1.0 (81 by 40 Field)

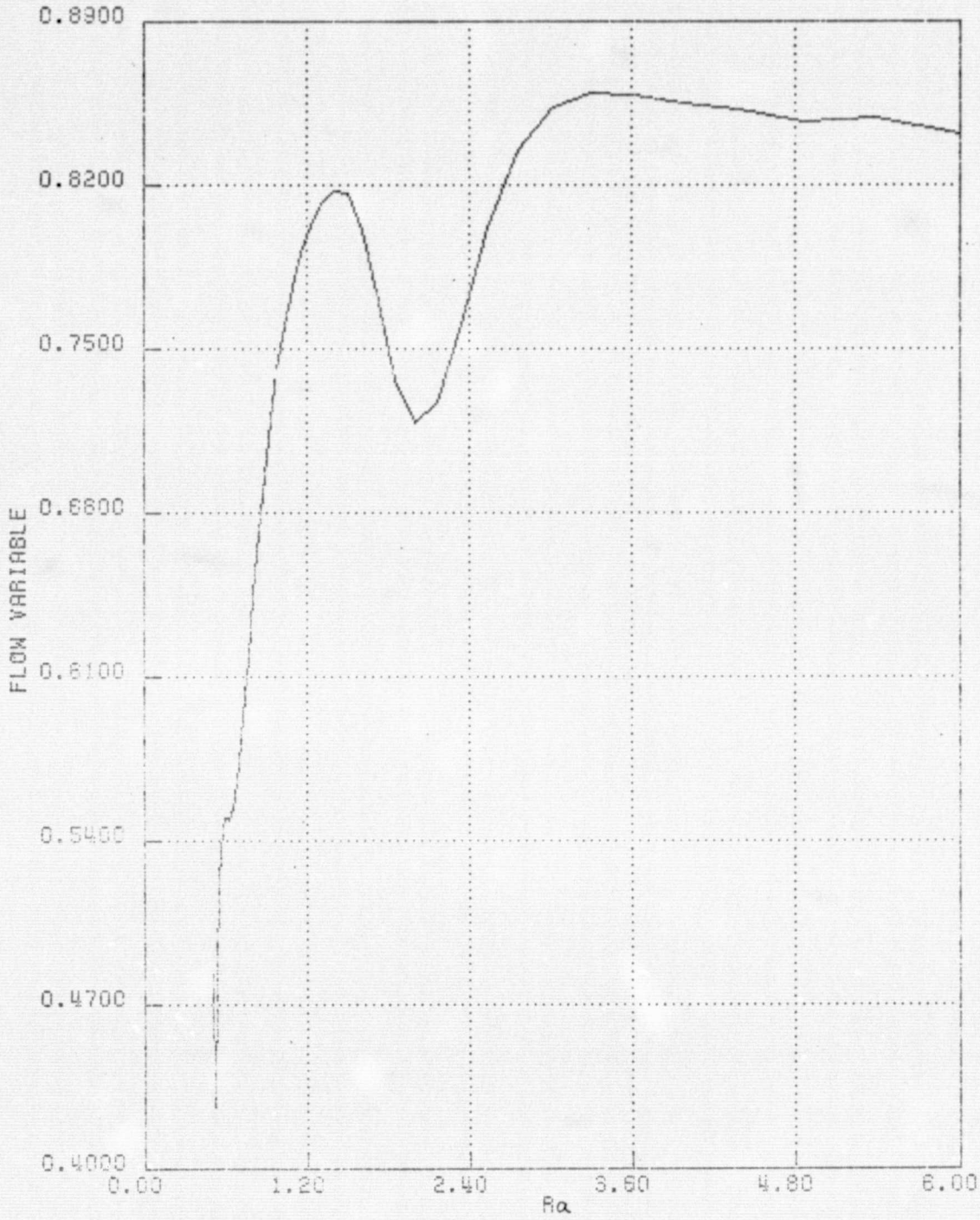

(b) Along ξ = 21 line

Figure 15b. Total Energy Profile with New Formulations at t = 1.0 (81 by 40 Field)

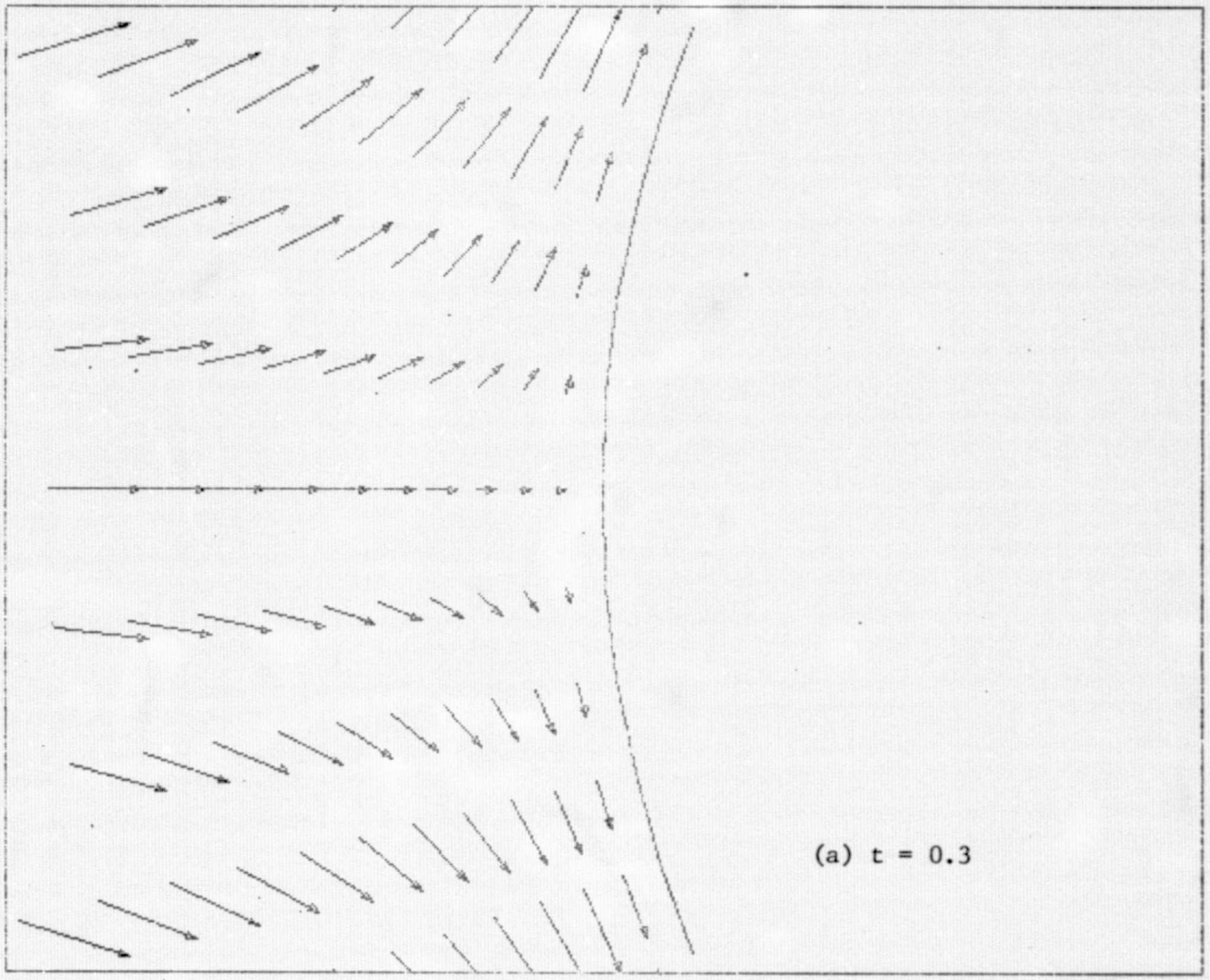

Figure 16a. Velocity Vectors near the Front Stagnation Point
(81 by 40 Field)

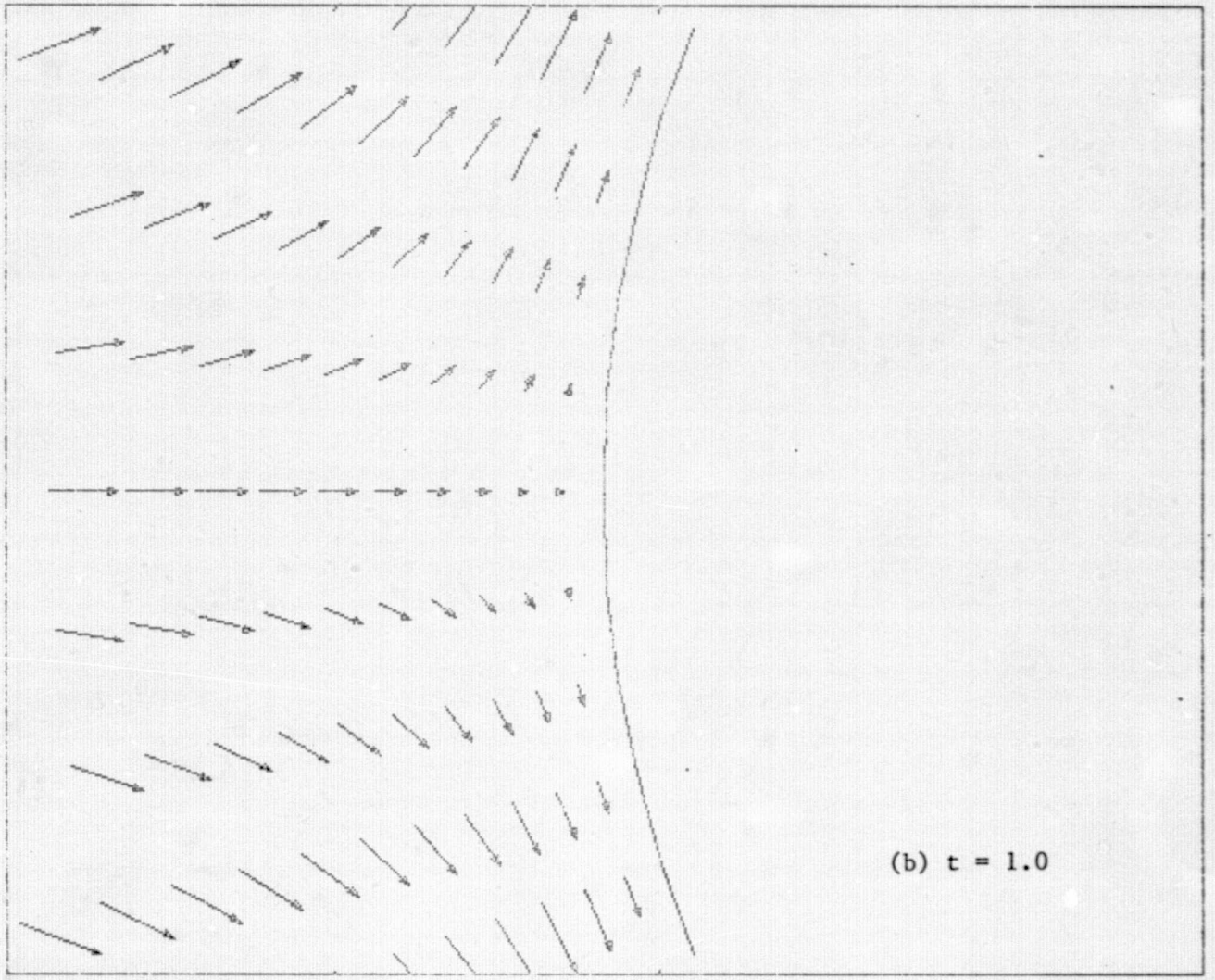

Figure 16b. Velocity Vectors near the Front Stagnation Point (81 by 40 Field)

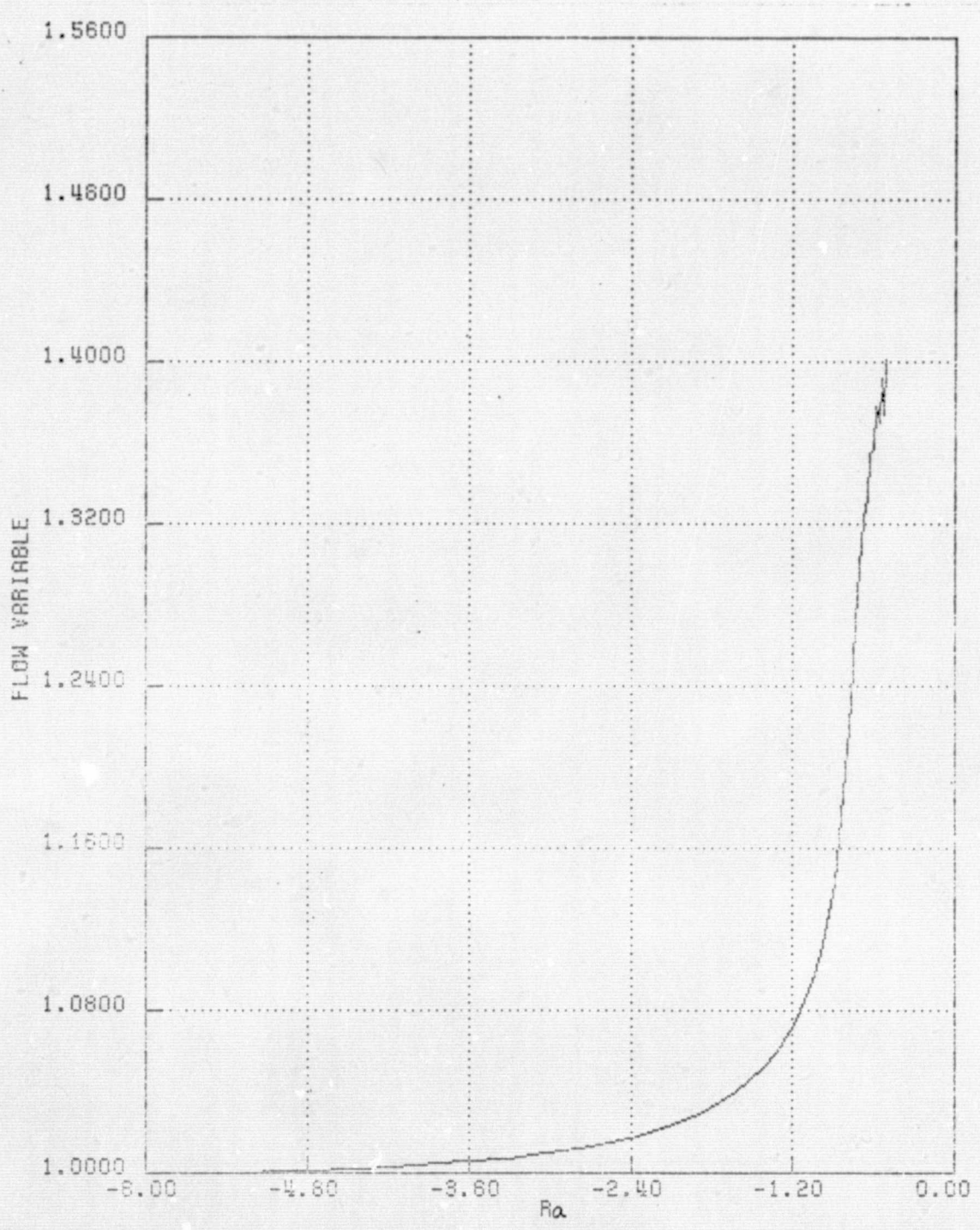

(a) Along ξ = 61 line

Figure 17a. Density Profile with Conventional Formulations at t = 0.3 (81 by 40 Field)

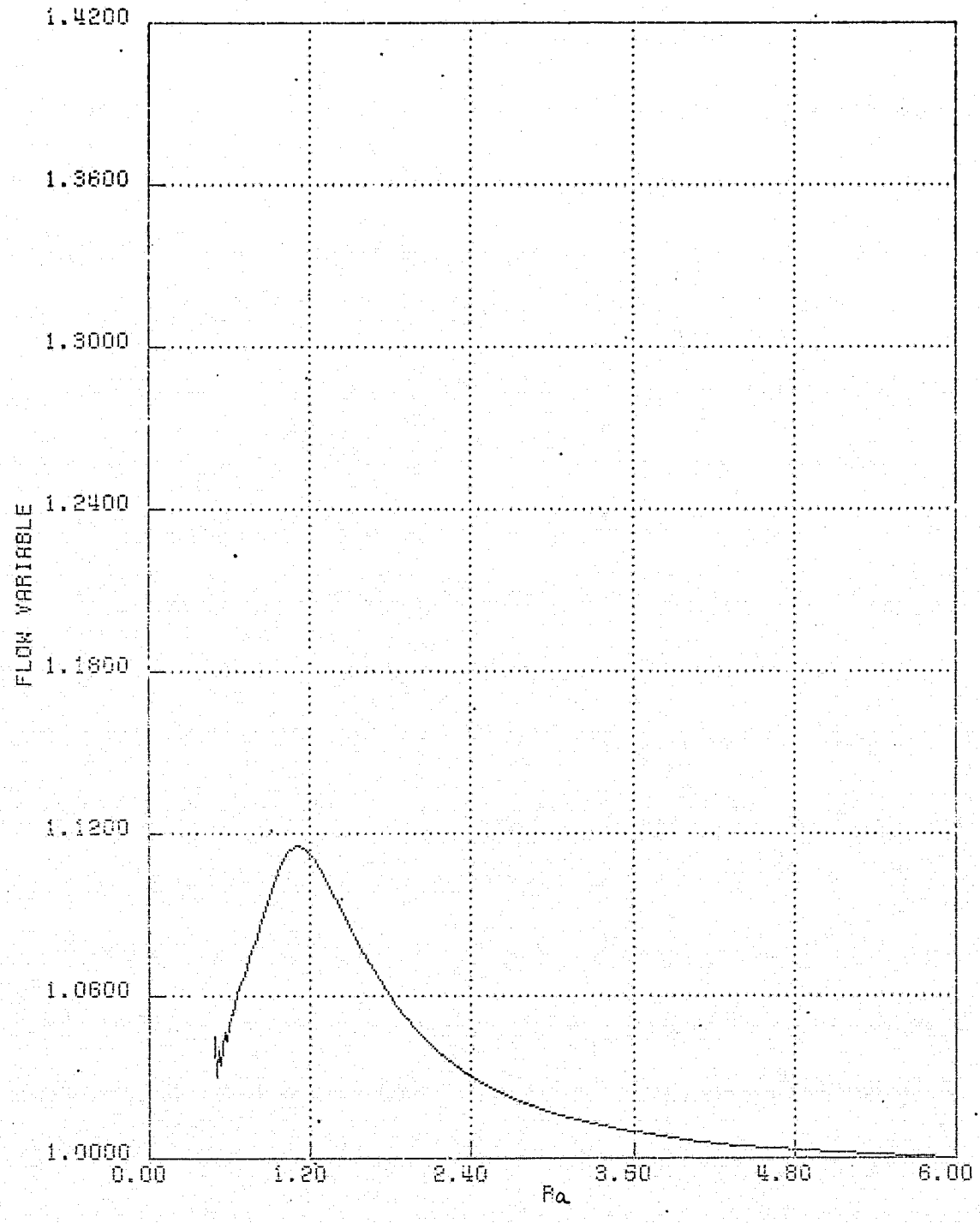

(b) Along ξ = 21 line

Figure 17b. Density Profile with Conventional Formulations at t = 0.3 (81 by 40 Field)

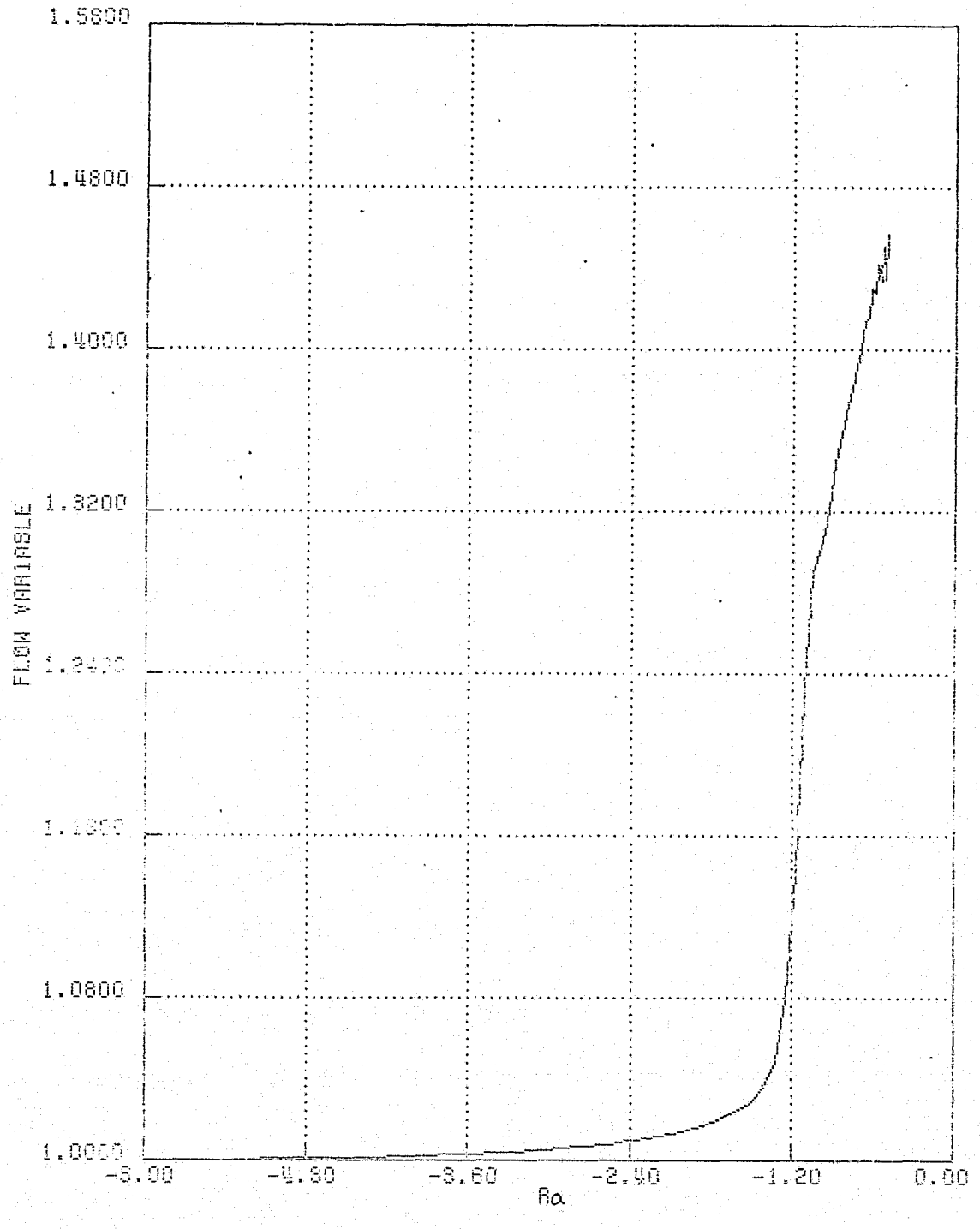

(a) Along ξ = 61 line

Figure 18a. Density Profile with Conventional Formulations at t = 1.0 (81 by 40 Field)

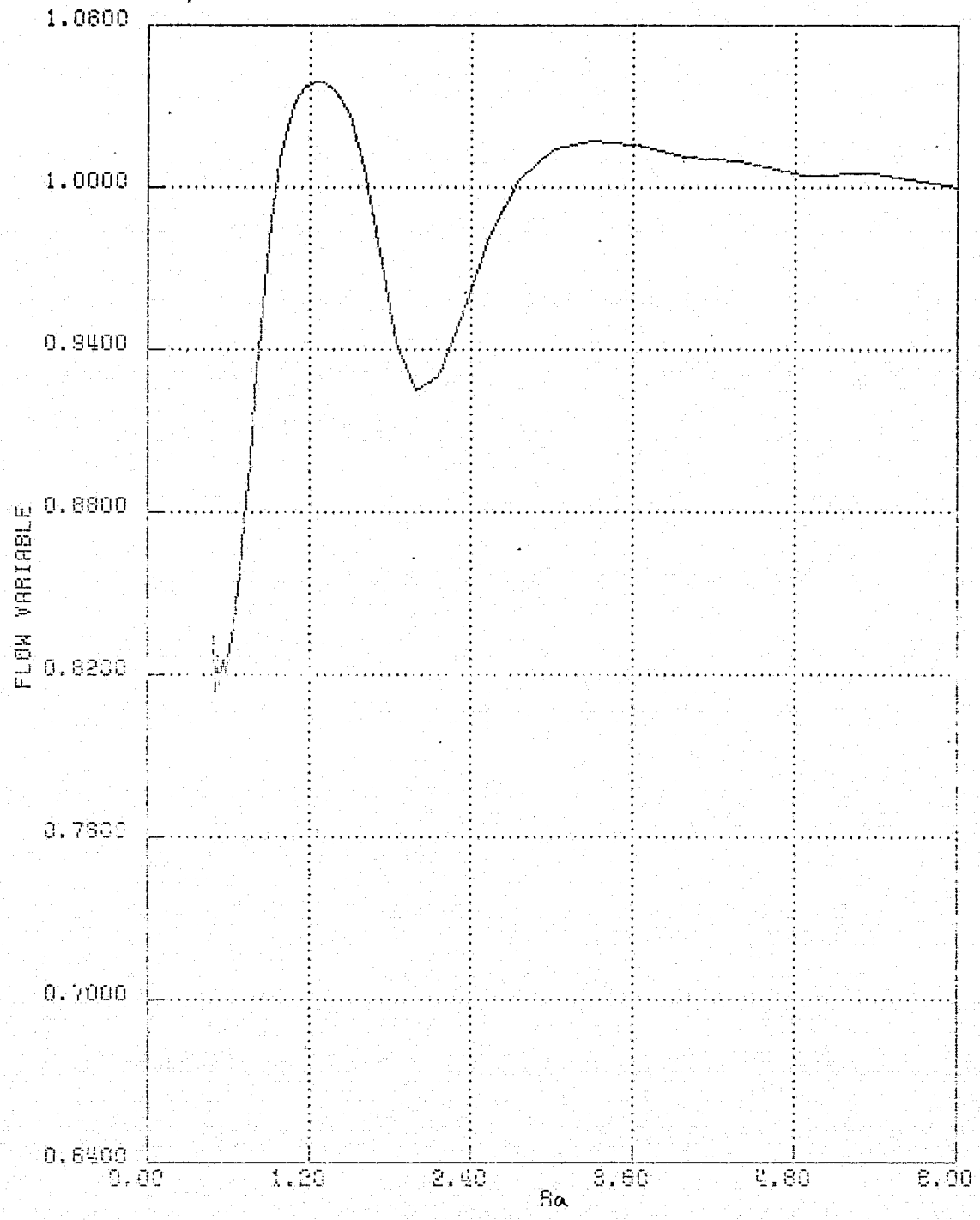

(b) Along ξ = 21 line

Figure 18b. Density Profile with Conventional Formulations at t = 1.0 (81 by 40 Field)

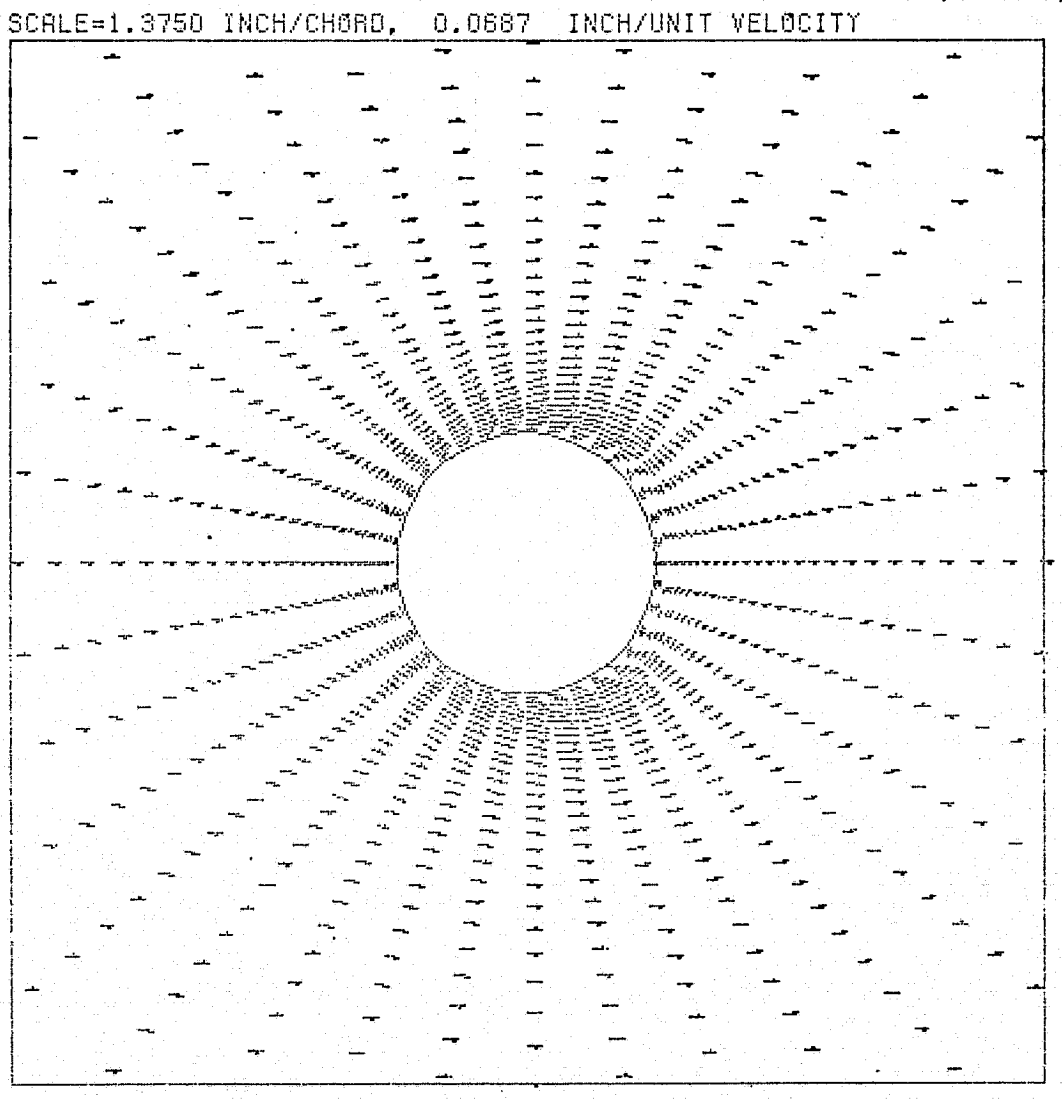

(a) t = 0.3

Figure 19a. Velocity Vectors with New Formulations on 37 by 40 Field

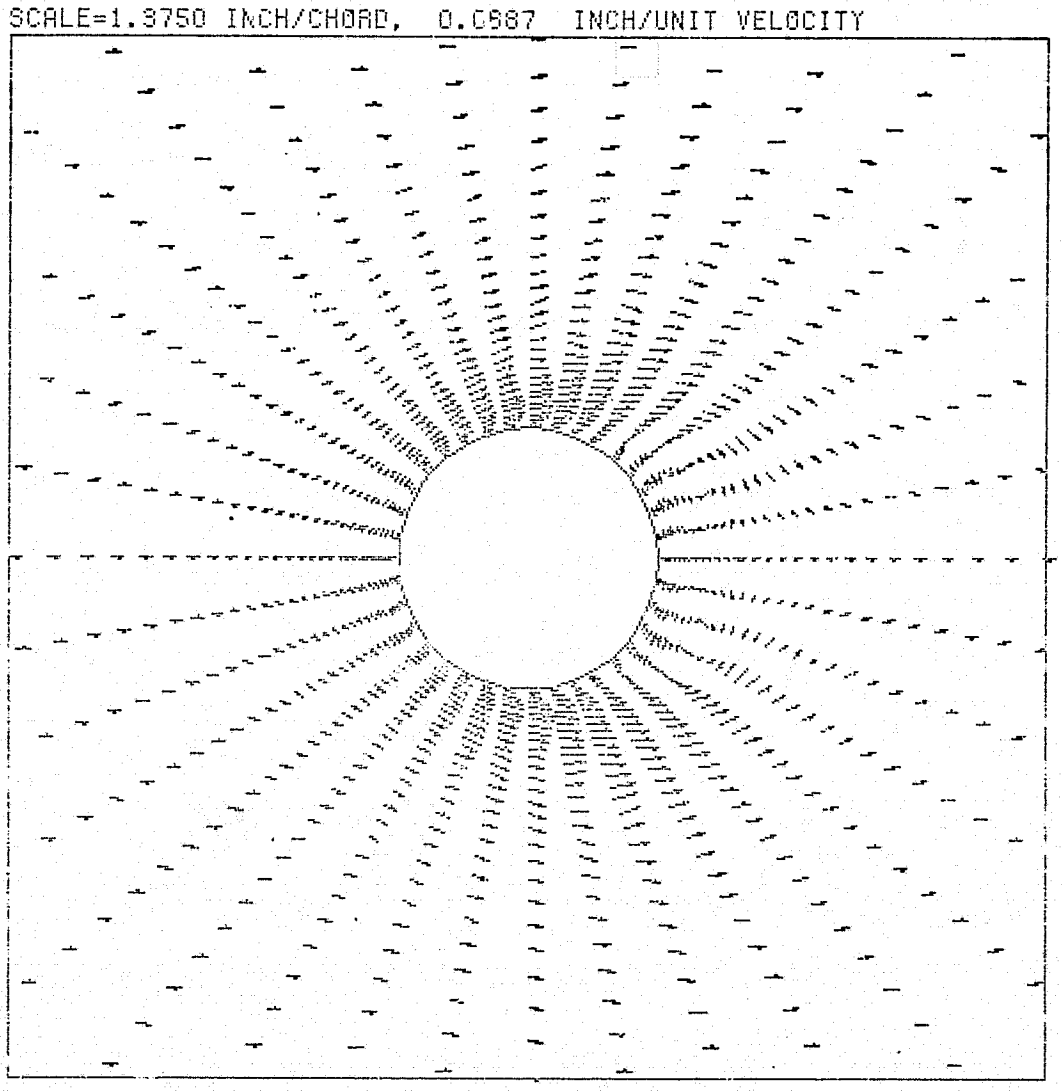

(b) t = 1.0

Figure 19b. Velocity Vectors with New Formulations on 37 by 40 Field

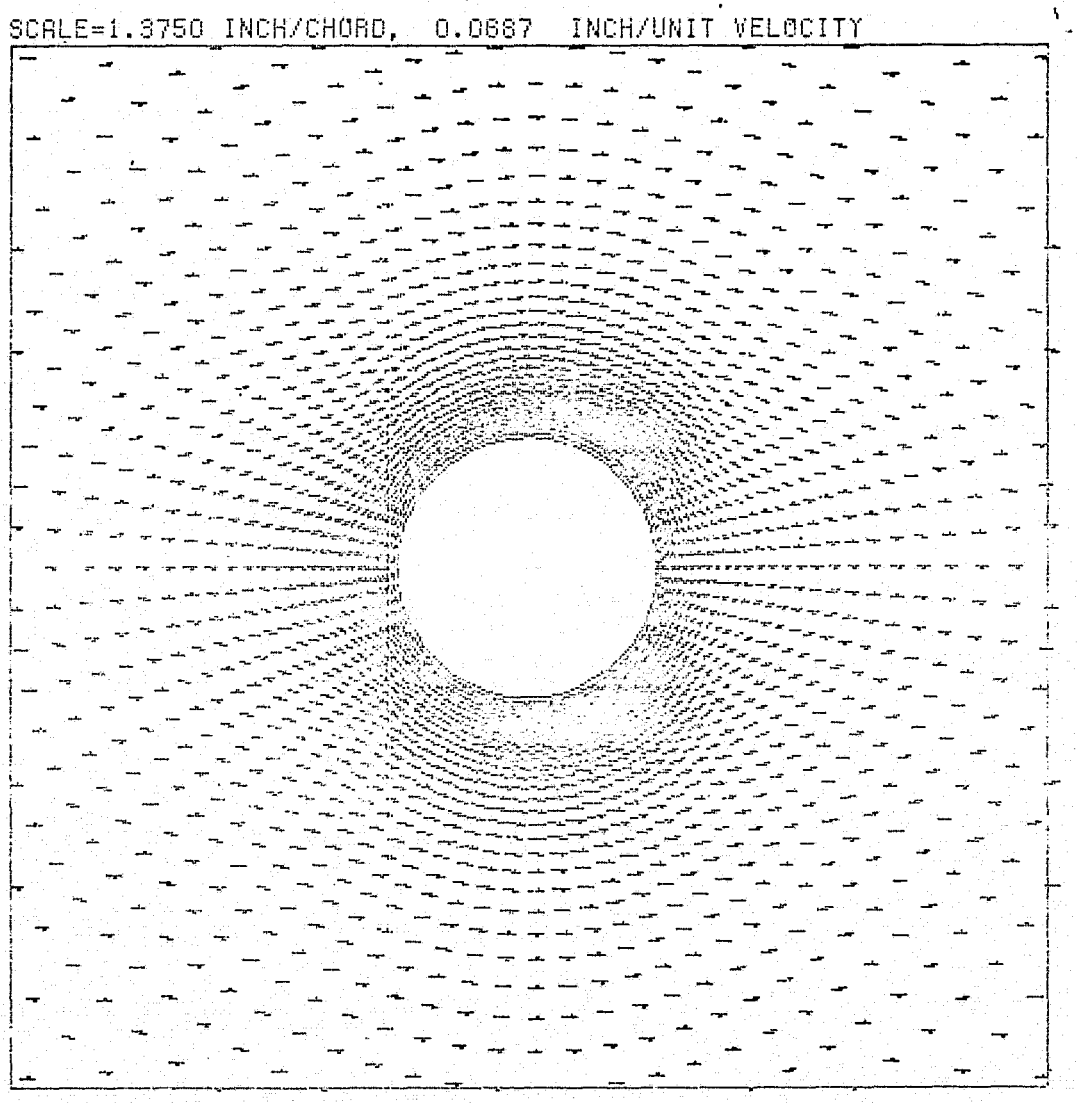

(a) t = 0.3

Figure 20a. Velocity Vectors with New Formulations on 81 by 40 Field

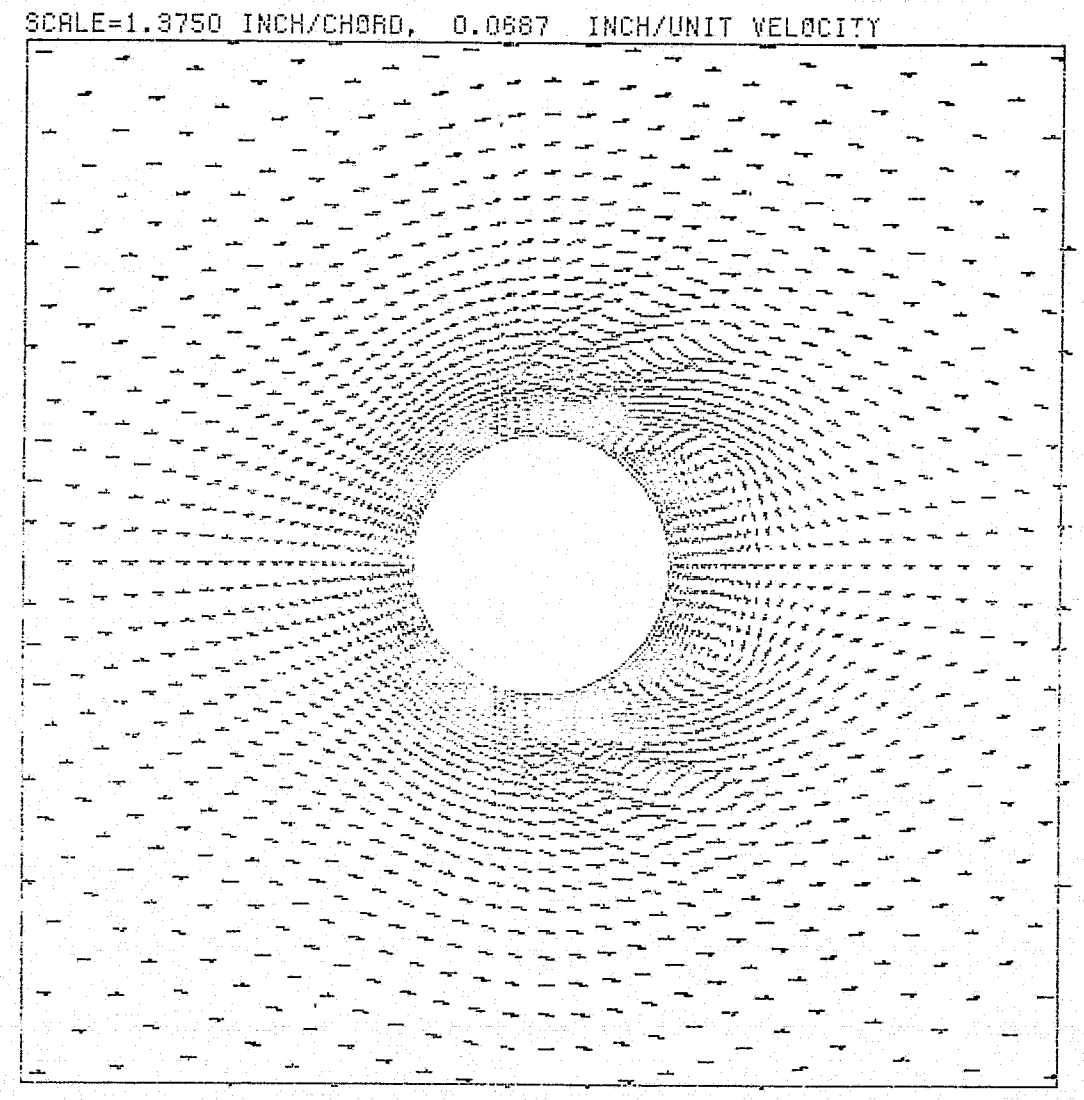

(b) t = 1.0

Figure 20b. Velocity Vectors with New Formulations on 81 by 40 Field

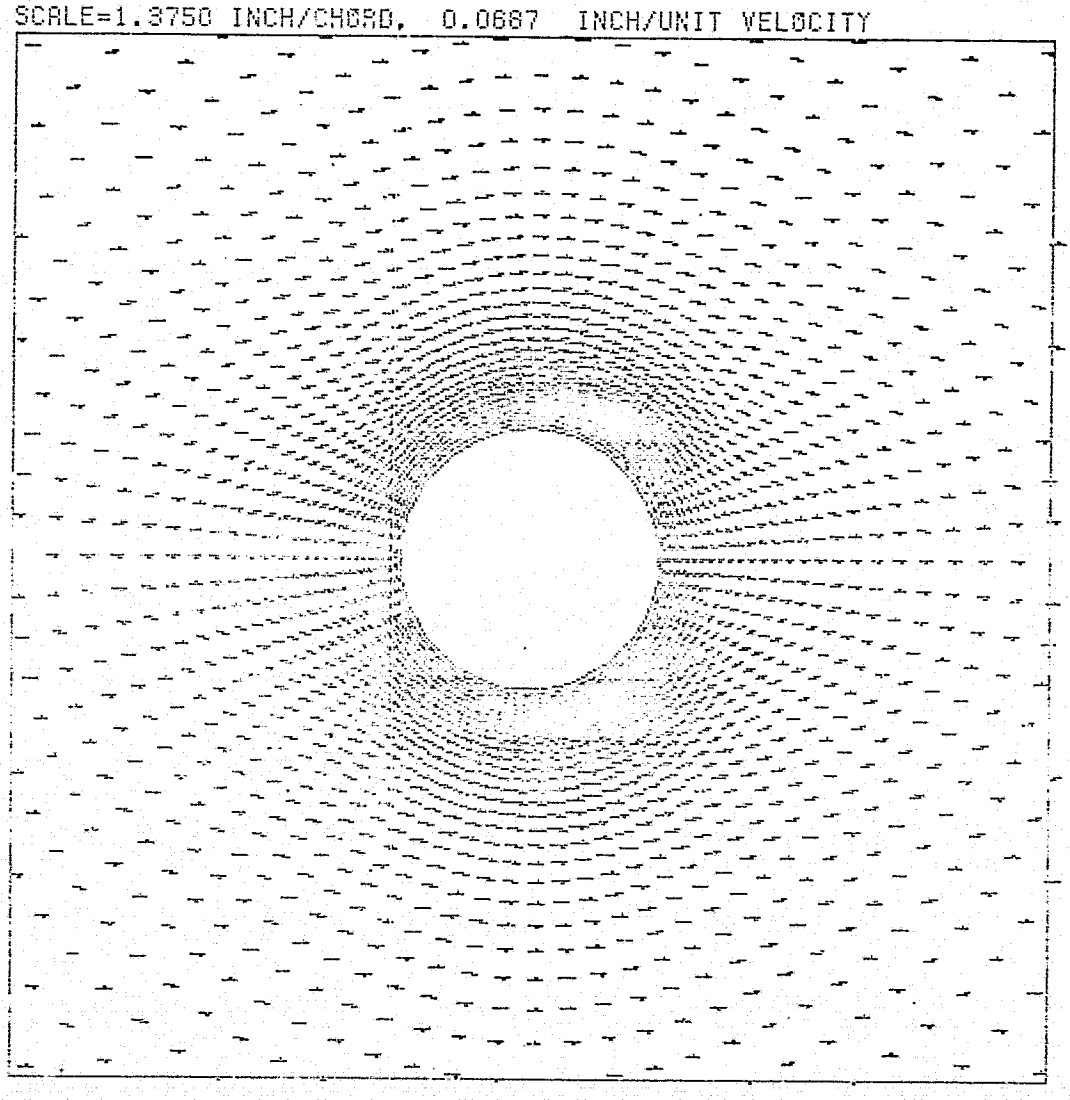

(a) t = 0.3

Figure 21a. Velocity Vectors with Conventional Formulations on 81 by 40 Field

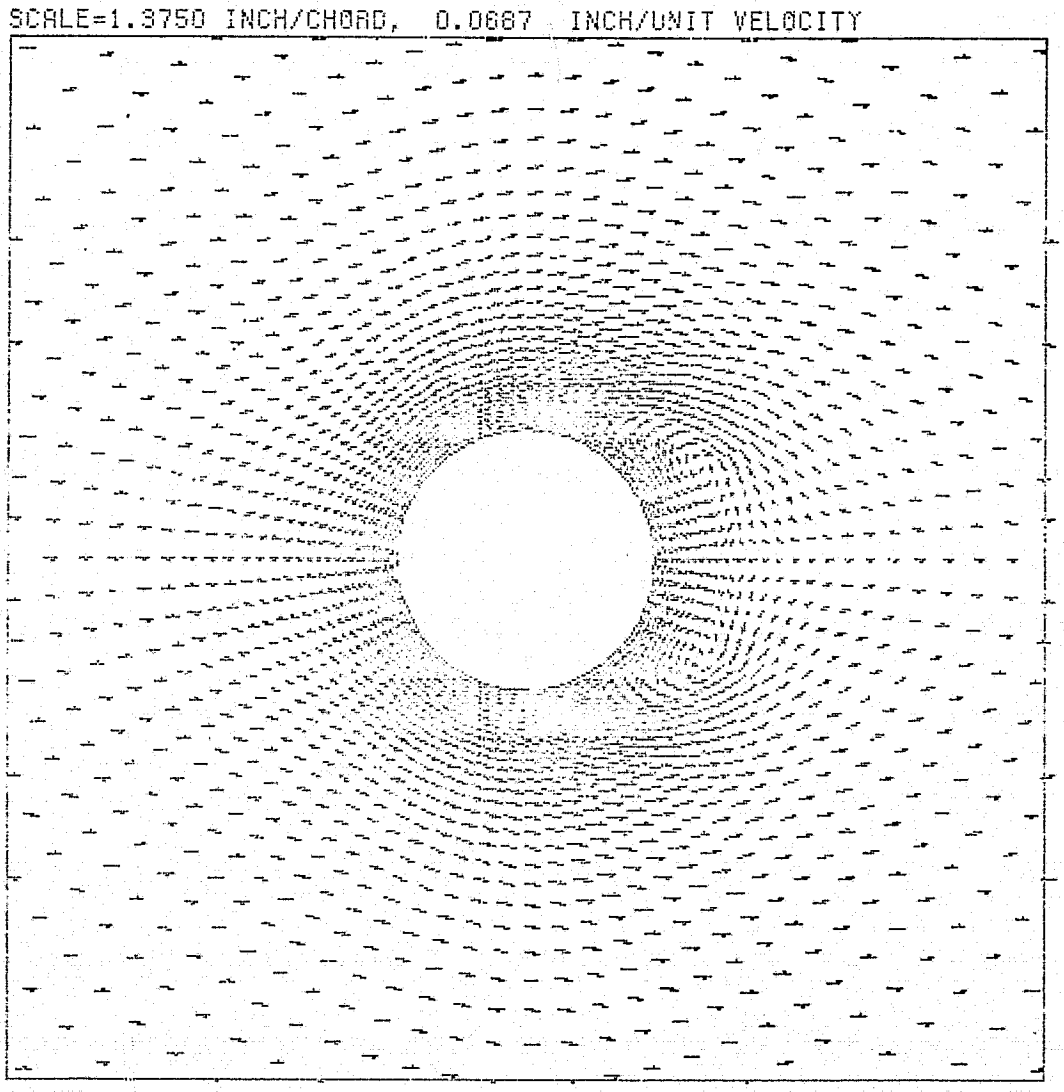

(b) t = 1.0

Figure 21b. Velocity Vectors with Conventional Formulations on 81 by 40 Field

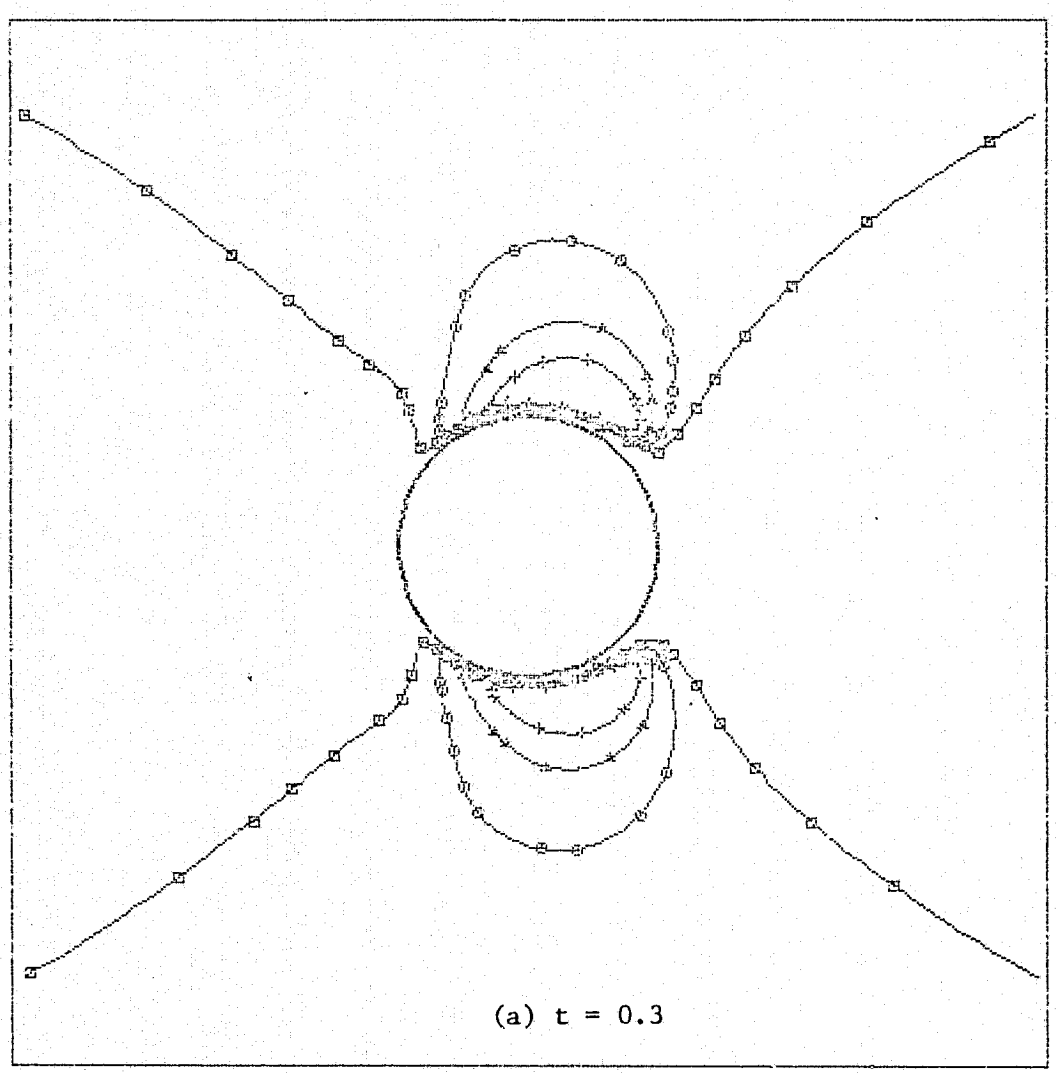

Figure 22a. Mach Number Contours with New Formulations on 81 by 40 Field

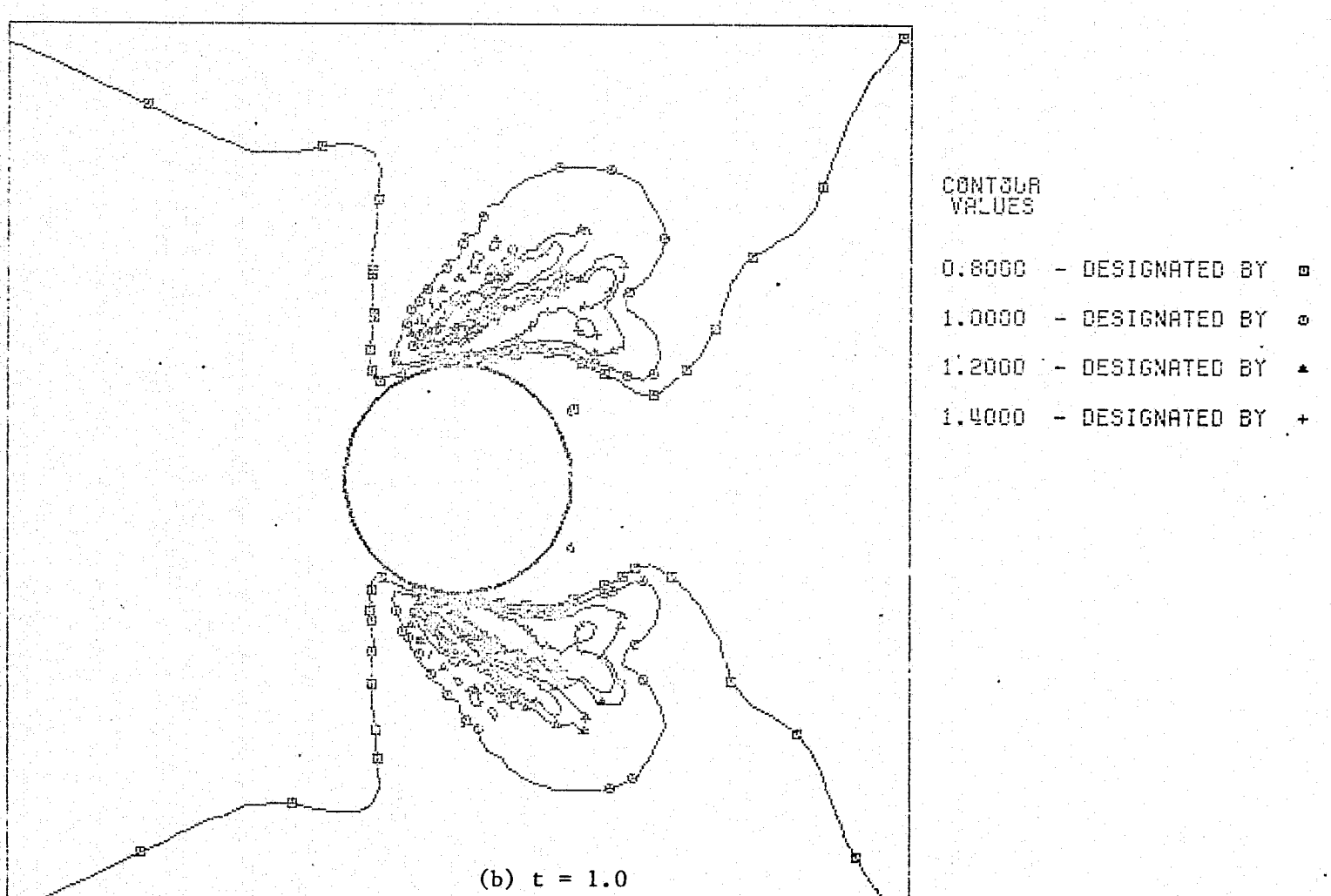

Figure 22b. Mach Number Contours with New Formulations on 81 by 40 Field

Figure 23. Isobars with New Formulations on 81 by 40 Field at t = 1.0

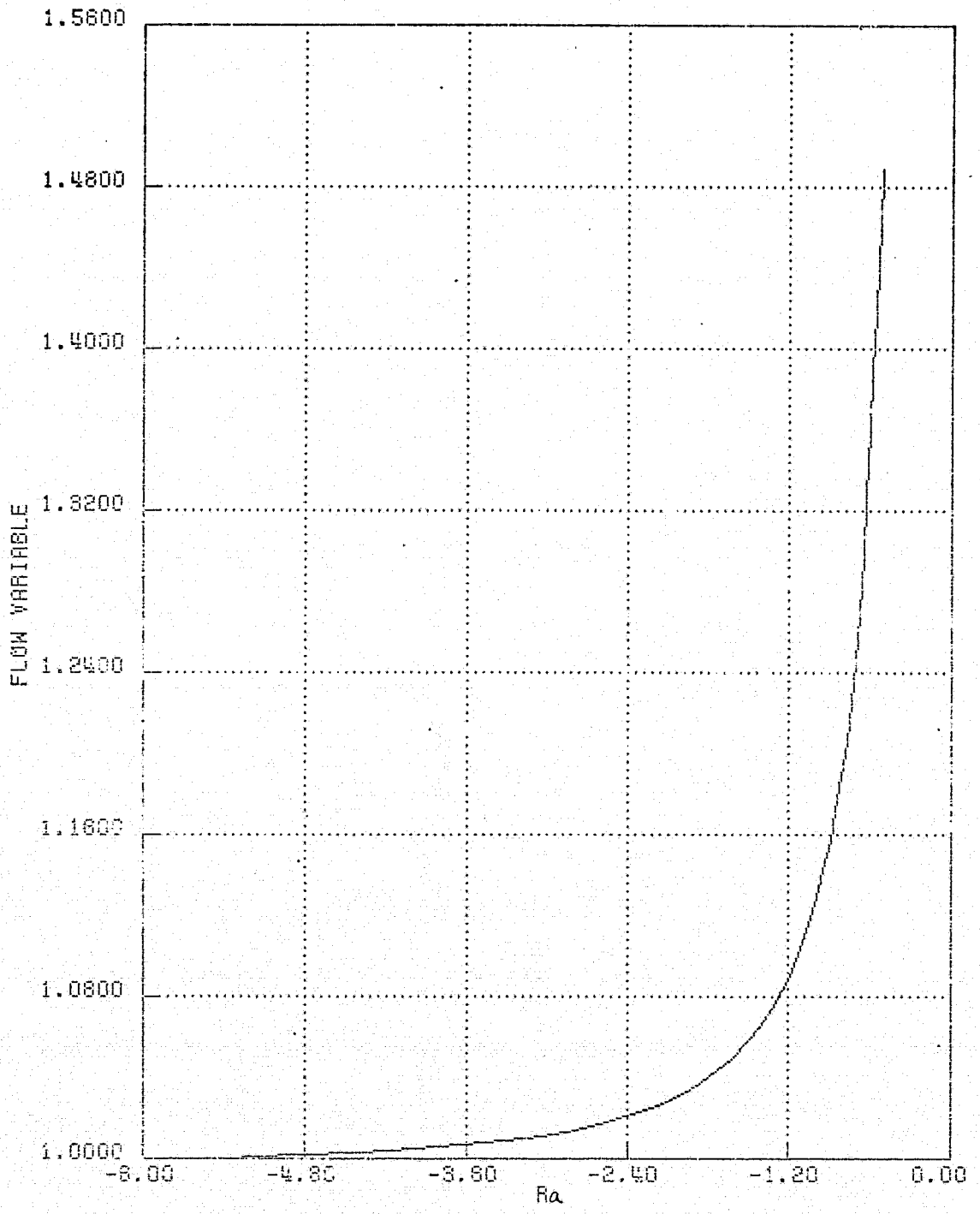

(a) Along ξ = 61 line

Figure 24a. Density Profile with R = 50 at t = 0.1 (81 by 40 Field)

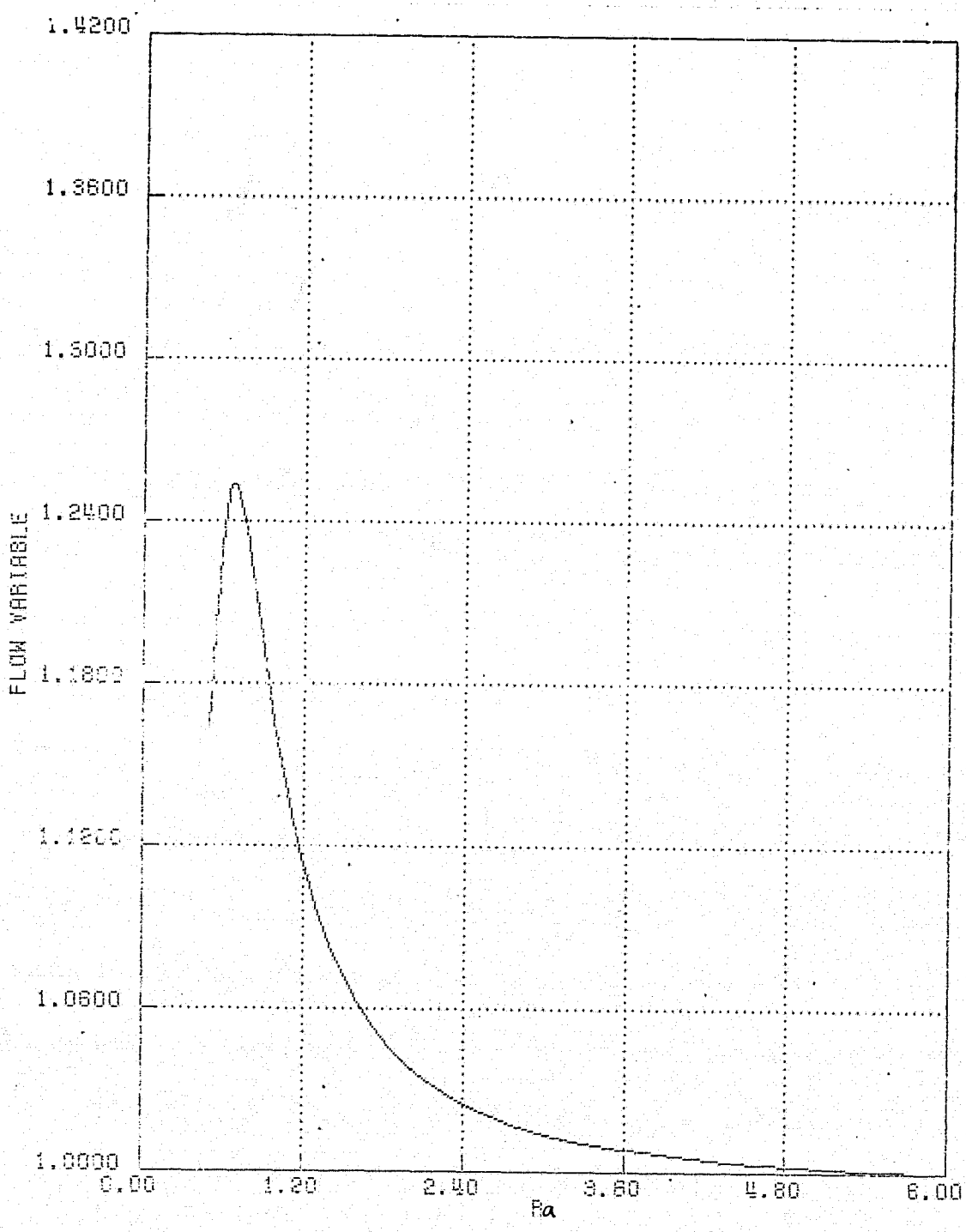

(b) Along ξ = 21 line

Figure 24b. Density Profile with R = 50 at t = 0.1 (81 by 40 Field)

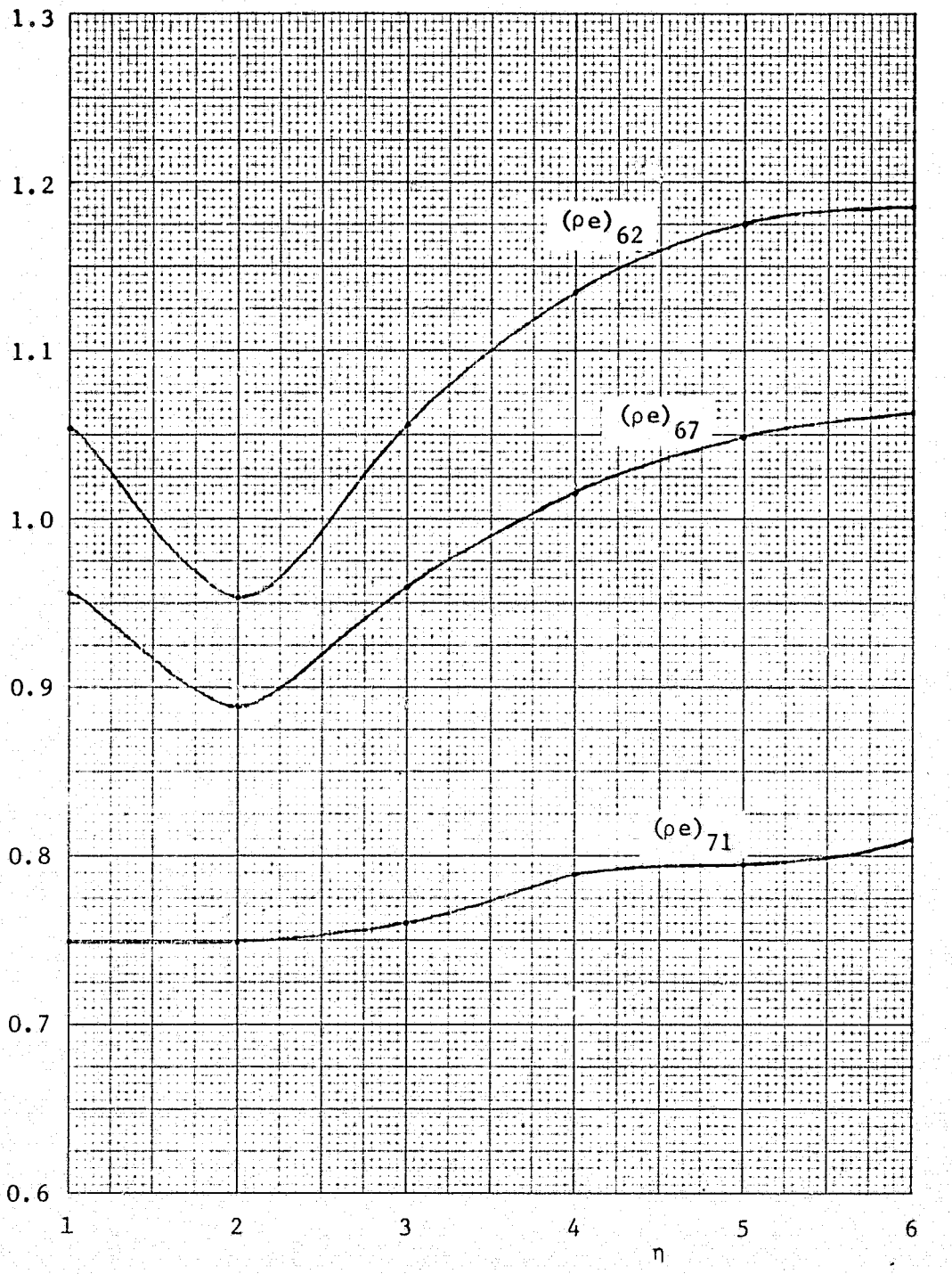

Figure 25. ρe Variations near the Wall

BIBLIOGRAPHY

1. Hamielec, A. E., and Raàl, J. D., "Numerical Studies of Viscous Flow around Circular Cylinders," The Physics of Fluid, January, 1969.

2. Kentzer, C. P., "Transonic Flows past a Circular Cylinder," Journal of Computational Physics, 6, 168 (1970)

3. Rajan, S., "A Parellel Algorithm for High Subsonic Compressible Flow over a Circular Cylinder," Journal of Computational Physics, 12, 534 (1973)

4. Thompson, J. F., Thames, F. C., and Mastin, C. W., "Boundary-Fitted Curvilinear Coordinate System for Solution of Partial Differential Equations on Fields Containing Any Number of Arbitrary Two-Dimensional Bodies," NASA CR-2729 (1977)

5. Thames, F. C., "Numerical Solution of the Incompressible Navier-Stokes Equations about Arbitrary Two-Dimensional Bodies," Ph.D. Dissertation, Mississippi State University, Mississippi State, Mississippi (1975)

6. Warsi, Z. U. A., and Thompson, J. F., "Machine Solutions of Partial Differential Equations in the Numerically Generated Coordinate Systems," Report MSSU-EIRS-ASE-77-1, Engineering and Industrial Research Station, Mississippi State University, (1976)

7. Thompson, J. F., Thames, F. C., and Mastin, C. W., "Automatic Numerical Generation of Body-Fitted Curvilinear Coordinate System for Field Containing Any Number of Arbitrary Two-Dimensional Bodies," Journal of Computational Physics, 15, 299 (1974)

8. Turner, L., Ph.D. Dissertation to appear, Mississippi State University (1978)

9. Schlichting, H., Boundary Layer Theory, McGrow-Hill sixth edition, 312 (1968)

10. Thompson, P. A., Compressible-Fluid Dynamics, McGrow-Hill, 30 (1972)

11. Thompson, J. F., Computer Routine BOFIT, Department of Aerophysics and Areospace Engineering, Mississippi State University.

12. Steger, J. L., and Lomax, H., "Transonic Flow about Two-Dimensional Airfoils by Relaxation Procedures," AIAA Journal, Vol. 10, No. 1 (1972)

13. Magnus, R., and Yoshihara, H., "Unsteady Transonic Flows over an Airfoil," AIAA Journal, Vol. 13, No. 12 (1975)

14. Hung, C. M., and MacCormack, R. W., "Numerical Solutions of Supersonic and Hypersonic Laminar Compression Corner Flows," AIAA Journal, Vol. 14, No. 4 (1976)

15. Deiwert, G. S., "Numerical Solutions of High Reynolds Number Transonic Flows," AIAA Journal, Vol. 13, No. 10 (1975)

16. Deiwert, G. S., "Recent Computation of Viscous Effects in Transonic Flow," Proceedings of the Fifth International Conference on Numerical Methods in Fluid Dynamics, Lecture Notes in Physics, 59, 159 (1976)